Slx8 Facilitates Loading of Rad51 at CAG Repeats in *Saccharomyces cerevisiae*

Anicka AbiChedid

Biology Senior Honors Thesis

Tufts University, May 2023

Advisor: Dr. Catherine Freudenreich
Committee Member: Dr. Mitch McVey
Research Mentor: Tyler Maclay

Table of Contents

Acknowledgements

"Anyone who has never made a mistake has never tried anything new."
—*Albert Einstein*

This project has been an immensely rewarding experience that has been a defining feature of my undergraduate education. I would like to first thank Dr. Catherine Freudenreich for granting me the opportunity to conduct research in her laboratory and offering me a space to explore a fascinating area of science. I have been incredibly fortunate to have her guidance and continued support throughout this project and my other endeavors. I would like thank Tyler Maclay, for being a phenomenal mentor and model scientist. I am very appreciative of his continued feedback, insights, and advice at every step of this project. A sincere thank you to Dr. Mitch McVey, who has served on my committee and has continuously been supportive of my endeavors. I have also had the pleasure of being a student in two of his classes and I am grateful to have had the opportunity to learn from him. I would also like to thank Dr. Mili Das, for being a mentor at the start of my project and teaching me many of the skills I needed to be successful in the lab. I am incredibly grateful for my fellow undergraduates in the lab as they have made my experience even more positive and enjoyable. The community that all the members of the Freudenreich laboratory have created is one that is collaborative, passionate, and driven, and I am thankful to have had such an amazing group of people to work with. Thank you to my parents and siblings for supporting my ambitions and always encouraging me to pursue my goals throughout my undergraduate years. An additional thank you to my partner, Tyler Hobart, who has offered his unwavering support, kindness, and compassion throughout every hardship. Lastly, I would like to thank the Russell L. Carpenter Fund for financially supporting my project and the NSF REU program at Tufts for allowing me to present my work during the summer of 2022. While I certainly have had my fair share of unsuccessful experiments and failures along the way, it has been an incredibly rewarding experience extending the boundaries of our scientific knowledge. I am so excited to be pursuing my Ph.D. in Cell and Molecular Biology at Duke University this fall. I am thrilled to have an opportunity to continue my journey in biological research and I could not have done it without all the people I have mentioned. Thank you very much.

Abstract

Repetitive DNA sequences in the genome have been shown to form alternative DNA structures and have been implicated in a variety of genetic diseases. The CAG trinucleotide repeat can form imperfect hairpin and slipped-strand structures, which is detrimental to DNA replication since the replisome has difficulty passing these barriers. Changes in the number of repeats within this region can occur during repair. Most notably, expansions in CAG repeat number are the cause of neurodegenerative diseases, like Huntington's disease and spinocerebellar ataxia, when they occur in the implicated gene. It has been previously shown that expanded CAG repeats relocate from the interior of the nucleus to the nuclear pore complex (NPC) for repair. The type of repair happening at the NPC is especially interesting to study since genome integrity is preserved and changes in repeat number are less likely to occur here. Movement of the repeats to the NPC is in part dependent on the SUMOylation state of other DNA repair proteins, and the Slx5-Slx8 complex plays an active role in regulating this movement. Interestingly, the Rad51 recombinase has been shown to load at the CAG repeats only after they relocate to the NPC. In this study, we assess the roles of three proteins, Slx8, Srs2, and Sgs1, in relation to the loading of Rad51 at CAG repeats. We used fluorescence microscopy to measure the colocalization instances of the Rad51 protein with the CAG repeat locus in the absence of each of these proteins. The results of these experiments suggest that Slx8 regulates Rad51 loading both before and after the CAG repeats relocate to the nuclear pores.

Introduction

Trinucleotide Repeats and their Role in Disease

Trinucleotide repeat sequences in the genome can form secondary structures including imperfect hairpins and slipped-strand structures (Figure 1; Ohshima & Wells, 1997). During DNA synthesis, these structures can stall replication fork progression (Ohshima & Wells, 1997; Pelletier et al., 2003; Samadashwily et al., 1997). Stalled replication forks are particularly unstable, and the cell often undergoes recombination events to resolve fork stalling and continue DNA synthesis, resulting in chromosomal rearrangements that are also characteristic of cancer cell genomes (Branzei & Foiani, 2005; Lambert et al., 2005). These expansions and contractions in repeat number are known as microsatellite instability. Notably, expanded trinucleotide repeats constitute fragile sites, which are locations of chromosomal breakage and result from failure to repair the fork stalling event (Freudenreich et al., 1998). Thus, it is critical that the cell repairs these DNA lesions to continue DNA replication and ensure cell viability.

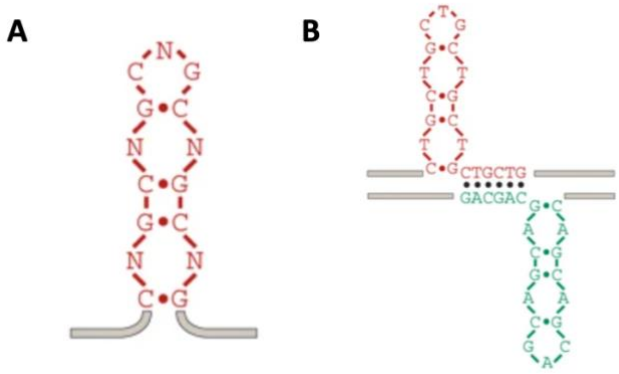

Figure 1. (A) Imperfect hairpin structure resulting from $(CNG)_n$ sequences. (B) Slipped-strand structure resulting from $(CAG)_n$ sequences. Adapted from Mirkin, 2007.

Repeat expansions in both coding and non-coding regions of the genome are implicated in a variety of neurodegenerative and neuromuscular diseases. CAG repeat expansions in the open reading frame of certain genes can result in disease including Huntington's disease and

spinocerebellar ataxia. In the disease state, 40 to 70 repeats of CAG are typically present whereas the non-disease causing range is typically 5 to 35 repeats (Reddy & Housman, 1997). Trinucleotide repeat expansions in non-coding regions of the genome can cause diseases that include myotonic dystrophy and fragile X syndrome. These repeat expansions can range from 50 repeats to thousands of repeats (Reddy & Housman, 1997). Disease progression and pathogenesis is exacerbated with larger repeat expansions (López Castel et al., 2010).

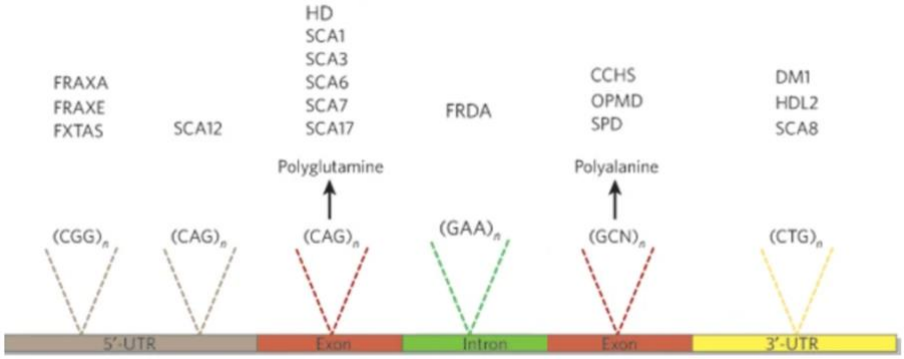

Figure 2. Expandable repeats located in specific regions of the genome can cause disease. $(CGG)_n$ sequences in the five prime untranslated regions (UTR) cause fragile X syndrome (FRAXA), fragile XE syndrome (FRAXE), and fragile X-associated tremor and ataxia syndrome (FXTAS). $(CAG)_n$ in the five prime UTR and coding regions of certain genes causes spinocerebellar ataxia (SCA) and Huntington's disease (HD). $(GAA)_n$ in a non-coding region causes Friedreich's ataxia (FRDA). $(GCN)_n$ in coding regions causes congenital central hypoventilation syndrome (CCHS), oculopharyngeal muscular dystrophy (OPMD), and synpolydactyly (SP). Finally, $(CTG)_n$ sequences in the three prime UTR cause myotonic dystrophy (DM), Huntington's disease-like 2 (HDL2), and SCA. Adapted from Mirkin, 2007.

The Role of SUMOylation in Maintaining Genome Integrity

SUMOylation is a post-translational modification that consists of multiple enzymatic processes. First, an inactivated SUMO molecule binds an E1 enzyme which activates SUMO through an ATP-dependent process (Johnson, 2004). The E1 enzyme passes activated SUMO to the highly conserved E2 enzyme Ubc9, which can act alone in SUMOylating its target, or is assisted by an E3 enzyme to conjugate SUMO to its target at a lysine residue (Branzei et al., 2006;

Johnson, 2004). In budding yeast, Mms21, Siz1, and Siz2 are the E3 SUMO-protein ligases. SUMOylation is a reversible process where the Ulp enzymes can cleave SUMO from its target and regenerate a SUMO that can be activated again by an E1 enzyme (Johnson, 2004). It is important to note that SUMO genes code for the SUMO protein precursor, and an additional function of Ulp enzymes is to cleave a C-terminal fragment from the precursor to generate mature SUMO (Johnson, 2004).

Rad51 is a recombinase that catalyzes strand-exchange during homologous recombination in an ATP-dependent manner (Kowalczykowski, 1998). The recombination pathway is associated with preserving genome integrity, however recombination events can also lead to contractions and expansions in repeat number (Jakupciak & Wells, 1999). SUMOylation can regulate recombination. One way this occurs is that Ubc9 and Siz1 mediated SUMOylation of PCNA recruits Srs2 which is a helicase that removes Rad51 filaments from single-stranded DNA, thereby preventing recombination events from occurring (Pfander et al., 2005). Another way this occurs is that the E3 SUMO ligase activity of Mms21 aids in preventing Rad51-dependent recombination events from occurring at stalled replication forks (Branzei et al., 2006).

The Slx5-Slx8 complex is heavily involved in the SUMOylation pathway due to its SUMO-targeted ubiquitin ligase (STUbL) function. This complex has been shown to negatively regulate both Rad51-dependent and Rad51-independent recombination events (Burgess et al., 2007). Specifically, cells lacking the Slx5-Slx8 complex exhibit increased Rad52-mediated recombination events (Burgess et al., 2007). The Slx5-Slx8 complex has also been shown to regulate the SUMOylation status of repair proteins involved in Rad51-independent recombination events. In the absence of Slx5 and Slx8, global SUMOylation levels of RPA, Rad52, and Rad59 decreased (Burgess et al., 2007).

Expanded CAG Repeats Relocate to the Nuclear Pore Complex

The nucleus has key domains, including the nuclear periphery and nuclear pores, where certain DNA repair processes occur. Chromatin can relocate to different areas of the nucleus for repair, depending on the type of DNA damage that is occurring. For example, double-strand breaks in DNA that are not quickly repaired through recombination with a nearby homologous template relocate to the nuclear periphery and are tethered to the Mps3p nuclear envelope protein (Oza et al., 2009). Eroded telomeres relocate to the nuclear pore complex (NPC) for repair and associate with the Nup133 nuclear pore protein (Khadaroo et al., 2009).

Expanded CAG repeats are also known to relocate to the NPC during late S phase (Su et al., 2015). Interestingly, in the absence of the Nup84 nuclear pore protein or the Slx5-Slx8 complex, increased fragility and instability is observed in the repeat tract (Figure 3). This is consistent with the idea that in the absence of the Nup84 protein, chromosomal rearrangements are often observed (Nagai et al., 2008). Additionally, the increased instability rate is suppressed in the absence of Rad52, indicating that relocation to the NPC reduces Rad52-mediated recombination events (Su et al., 2015). Thus, movement of expanded repeats to the NPC serves to preserve genome integrity by avoiding recombination events, with Nup84 and Slx5-Slx8 being important proteins involved in promoting genome stability.

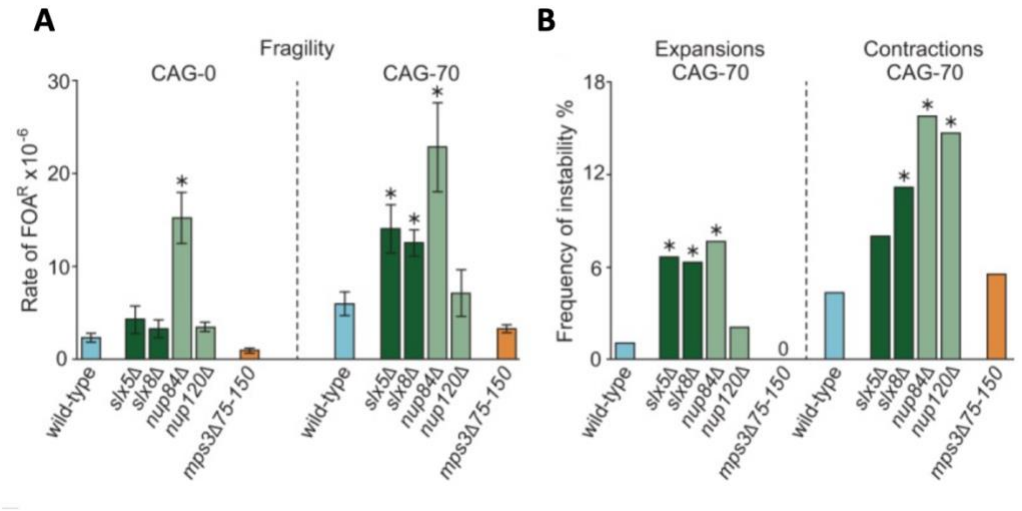

Figure 3. Fragility and instability in CAG repeat strains. (A) In the absence of Slx5, Slx8, and Nup84, fragility at the CAG-70 locus increased as compared to CAG-0. (B) Overall instability at the CAG-70 locus increased in the absence of Slx5, Slx8, and Nup84. Expansions were observed at the CAG-70 locus in the absence of Slx5, Slx8, and Nup84. Contractions were observed in the absence of Slx8, Nup84, and Nup120. Adapted from Su et al., 2015.

Requirements for Relocation of Expanded Repeats to the NPC

There are several conditions that must be met for expanded repeats to relocate to the NPC. The Slx5 protein is required for relocation and specifically serves in tethering the repeat to the nuclear pore (Su et al., 2015). Resection by either or both the Sgs1 helicase or Exo1 nuclease are needed for relocation, with the likely function of resection being to provide a single-stranded DNA platform to which single-stranded binding proteins like Rad51 and RPA can bind (Whalen et al., 2020). The exonuclease function of Mre11 is needed which acts upstream of the Sgs1 and Exo1 resection factors (Whalen et al., 2020). Finally, Mms21-mediated SUMOylation of Rad52, Rad59, and RPA is required for relocation to occur (Whalen et al., 2020). Consistent with the idea that relocation to the NPC preserves genome integrity by minimizing recombination events, both Rad51 and Rad52 recombination proteins are not required for relocation to occur (Su et al., 2015).

In fact, Rad52 is SUMOylated and targeted for degradation by the Slx5-Slx8 complex at the NPC (Su et al., 2015).

Mechanism of Relocation and Current Model

In the current model for relocation to the NPC, expanded repeats induce a fork stalling event that recruits Mre11 and Exo1 to resect DNA near the repeat, providing a single-stranded DNA platform to which RPA can bind (Figure 4C; Whalen et al., 2020). This event additionally recruits the Smc5-Smc6 complex, which facilitates Mms21-mediated SUMOylation of RPA. RPA-SUMO specifically excludes Rad51 from the repeat. These events facilitate the relocation of the replication fork to the NPC where the repeat is bound to the pores via the Slx5 SUMO-interacting motifs. The Mre11, Smc5, Rfa1, and Slx5 proteins are bound at the repeat prior to relocation. In contrast, Rad51 is excluded from the repeat tract while at the interior of the nucleus, and associates at the repeats only after relocation to the NPC (Figure 4A). Specifically, the percent colocalization of Rad51 with the replication fork before relocation is 5.6%, and after relocation is 58%, as reported in Whalen et al., 2020. SUMOylation of the Rfa1, Rfa2, and Rfa3 subunits of RPA is required for Rad51 exclusion, therefore RPA-SUMO may inhibit Rad51 from loading prematurely at the fork (Figure 4C; Whalen et al., 2020).

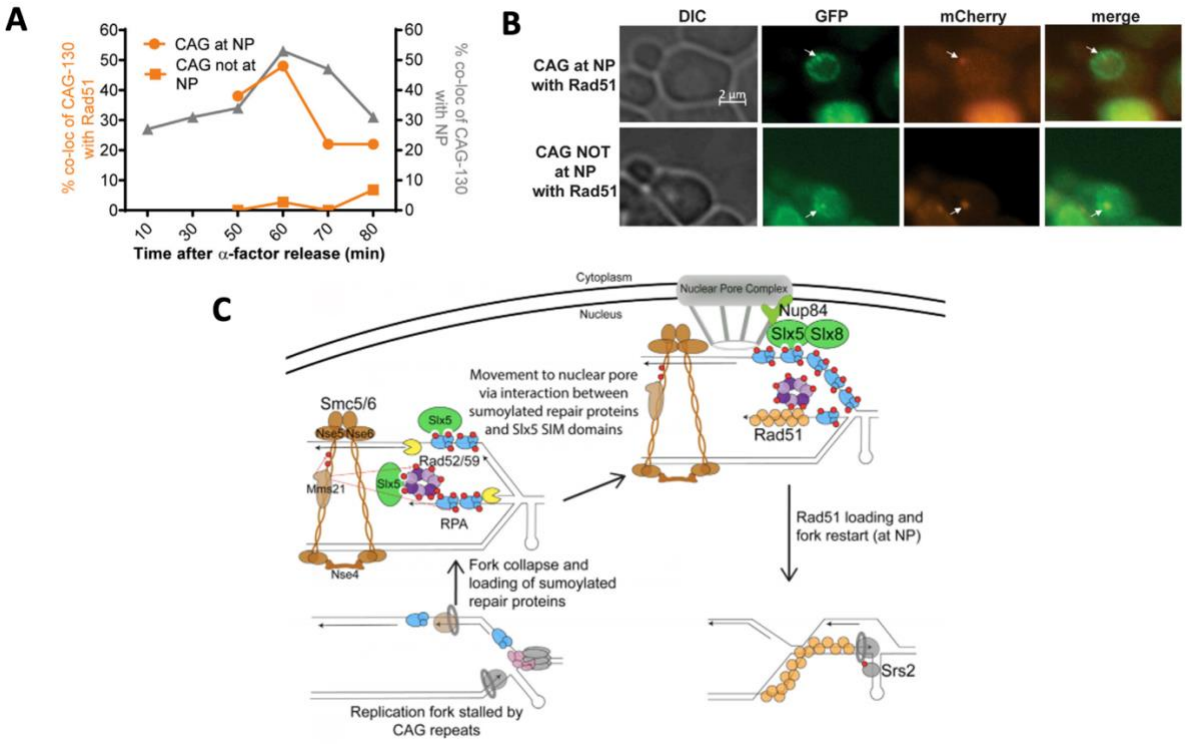

Figure 4. (A) Time-course of Rad51 colocalization with the CAG repeat across S-phase. (B) Example microscopy images depicting scoring of the colocalization in Whalen et al., 2020. (C) Model for replication fork relocation to the NPC. Upon a fork stalling event induced by CAG repeats, Smc5-Smc6 facilitates SUMOylation of DNA repair proteins by Mms21. SUMOylated repair proteins load and the replication fork relocates to the NPC. RPA-SUMO is not observed at the fork while at the NPC and Rad51 is loaded. It is suggested that afterwards, a fork restart mechanism is initiated. All parts of this figure reprinted from Whalen et al., 2020.

Hypothesis 1: RPA-SUMO is Degraded by Slx8 to Facilitate Rad51 Loading

It is known that RPA-SUMO directly inhibits Rad51 loading prior to the repeat relocating to the NPC (Whalen et al., 2020). However, it is unknown which proteins facilitate Rad51 loading after the repeat relocates to the pores. We hypothesized that RPA-SUMO needs to be removed to allow a single-stranded platform to which Rad51 can bind. It is known that Rad52-SUMO is targeted by Slx5-Slx8 for degradation, so it is possible that the Slx8 protein targets RPA-SUMO for degradation, after which it is removed from the fork through a process mediated by Cdc48, a protein that disassembles other protein complexes (Figure 5; Twomey et al., 2019).

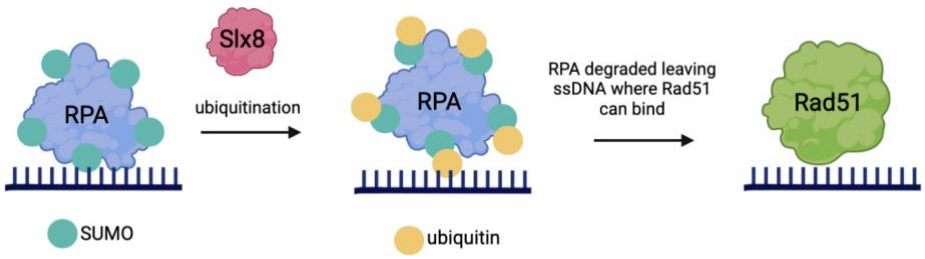

Figure 5. RPA-SUMO could be removed via ubiquitination by Slx8 at the NPC, initiating the Cdc48-mediated degradation process. After RPA-SUMO is removed, it would leave a single-stranded platform to which Rad51 can load. Figure created with BioRender.com.

Hypothesis 2: Srs2 Facilitates Rad51 Loading while at the NPC

However, it is also possible that factors other than Slx8 facilitate Rad51 loading at the NPC. For example, Srs2 works to prevent recombination events by stimulating ATP-hydrolysis within Rad51 nucleoprotein filaments, resulting in Rad51 dissociation from DNA (Antony et al., 2009). Srs2 has a SUMO-interacting motif (SIM) domain that binds SUMO and therefore can be recruited by other SUMOylated replication factors (Kolesar et al., 2012). Therefore, it is possible that Srs2 is recruited by RPA-SUMO and prevents Rad51 filaments from forming at the fork while at the interior of the nucleus (Figure 6A). Further, Srs2 has also been shown to disassemble RPA units from DNA, since loss of Srs2 in the cell led to an accumulation of RPA on chromatin (Dhingra et al., 2021). RPA might be deSUMOylated by Ulp1 at the NPC, after which it is stripped off by Srs2 (Figure 6B). This would leave a single-stranded platform to which Rad51 can load at the NPC. Alternatively, Srs2 is SUMOylatable at its lysine residues by the Siz factors, and therefore could be SUMOylated and targeted for degradation by a STUbL, such as Slx8 (Figure 6C; Kolesar et al., 2012). Removal of Srs2 at the NPC would then allow for Rad51 loading.

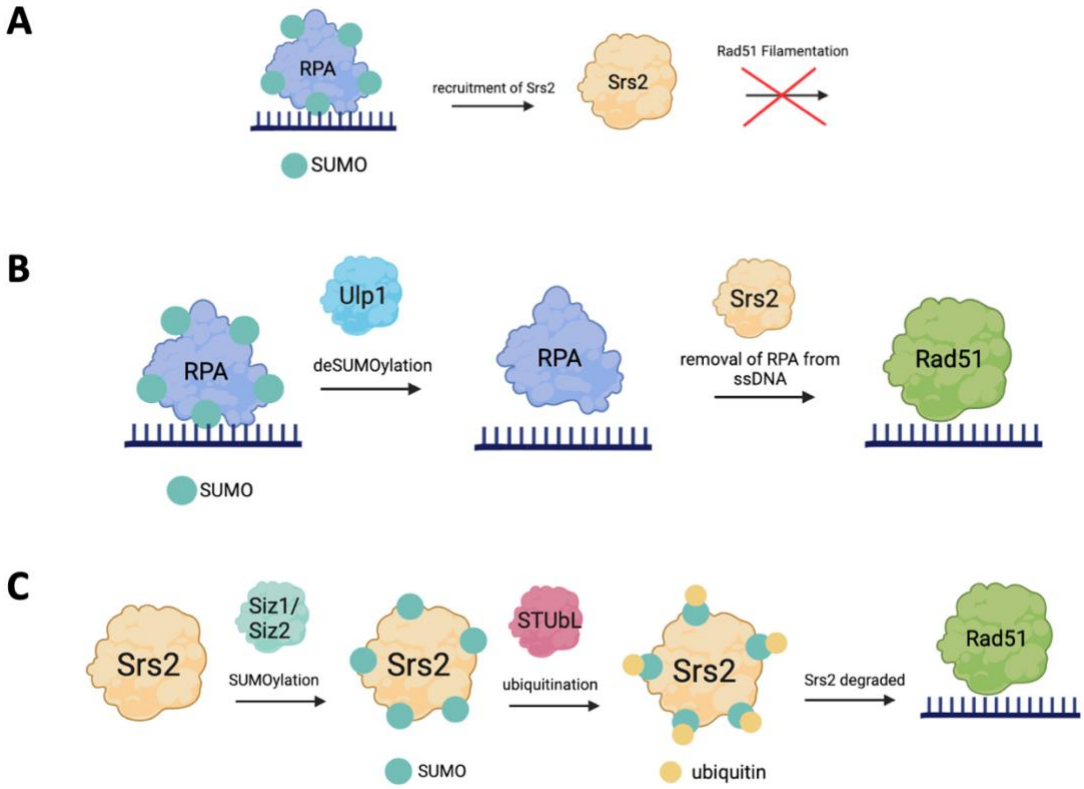

Figure 6. Two potential mechanisms by which Srs2 could facilitate Rad51 loading while at the NPC. (A) (B) RPA-SUMO is first deSUMOylated by Ulp1 after which it is removed by Srs2. This leaves a single-stranded platform to which Rad51 can load. (C) Alternatively, Srs2 is degraded by being SUMOylated and then ubiquitinated. When Srs2 is degraded, it no longer prevents Rad51 filamentation, and therefore Rad51 can load at the replication fork. Figure created with BioRender.com.

Hypothesis 3: Sgs1 Facilitates Rad51 Loading while at the NPC

Another possible factor facilitating Rad51 loading is the helicase activity of Sgs1, which is similar to Srs2 but has a fundamentally distinct role in DNA repair mechanisms. Sgs1 can be recruited to single-stranded DNA coated in both RPA and Rad51 (Crickard et al., 2019). While Sgs1 has been shown to disrupt Rad51 filament formation, it has not been shown to disassemble RPA units from chromatin. Additionally, Sgs1 interacts preferentially with the SUMOylated form of Rfa1, a subunit of RPA (Dhingra et al., 2019). Therefore, it is possible that RPA-SUMO recruits Sgs1 while the replication fork is at the interior of the nucleus, which would promote disassembling

of Rad51 prior to fork relocation (Figure 7A). The Slx5-Slx8 complex does not regulate the majority of Sgs1 protein levels within the cell via ubiquitination of Sgs1-SUMO and subsequent degradation (Böhm et al., 2015). However, the Slx5-Slx8 complex was shown to decrease Sgs1 focus formation, indicating that it may regulate Sgs1 function in a manner alternative to the degradation pathway or that the complex only targets Sgs1 proteins at the replication fork. Therefore, it is also plausible that the Slx5-Slx8 complex may facilitate degradation of Sgs1 proteins after the fork relocates to the NPC, which would allow for Rad51 loading in the absence of Sgs1 (Figure 7B).

Figure 7. Potential mechanism by which Sgs1 could facilitate Rad51 loading. (A) Before the replication fork relocates to the NPC, RPA-SUMO recruits Sgs1 which prevents Rad51 filamentation. (B) After the replication fork relocates to the NPC, Sgs1 is SUMOylated and then ubiquitinated, initiating the degradation process. Once Sgs1 is degraded, Rad51 filaments can form at the replication fork. Figure created with BioRender.com.

Purpose and Approach

The goal of this study was to determine which proteins are involved in facilitating Rad51 loading when a damaged replication fork is at the nuclear pores. Using the model organism *Saccharomyces cerevisiae*, we used fluorescence microscopy to locate the repeat locus, the Rad51 protein, and the NPC in late S-phase cells. To visualize the nuclear pore proteins, the Nup49 nuclear pore protein was endogenously tagged with the red fluorescent protein mCherry. The Rad51 protein was tagged with the yellow fluorescent protein mVenus on a plasmid. Finally, the

CAG repeat locus is visualized by fluorescently tagging the LacI repressor, a DNA binding factor that specifically binds the *lacO* target sequence (Robinett et al., 1996). 256 copies of the *lacO* target sequence are positioned 6.4 kilobases away from the CAG repeat sequence to form the *lacO* array. The LacI protein was N-terminally tagged with cyan fluorescent protein (CFP). This fluorescent protein then binds the array to produce a fluorescent focus to locate the approximate position of the CAG repeat locus in the cell.

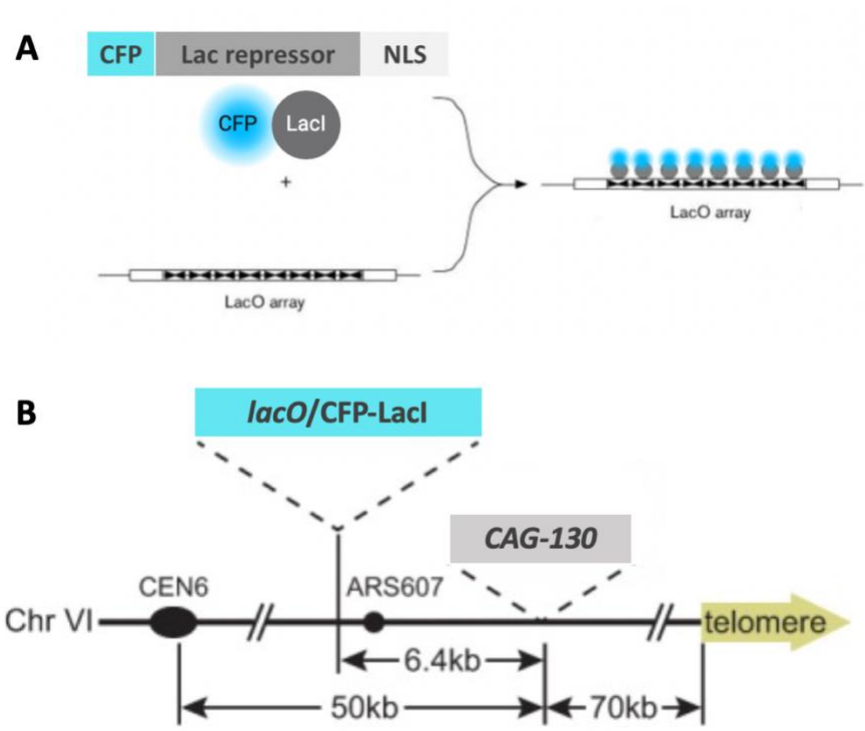

Figure 8. Mechanism for locating the CAG repeat locus using fluorescence microscopy. (A) LacI is N-terminally tagged with CFP to create a fluorescent fusion protein that binds to the *lacO* sequence. The NLS sequence targets this protein to the nucleus. There are 256 copies of the *lacO* sequence within the array, generating a robust fluorescent signal. Adapted from Straight et al., 1996. (B) Organization of *lacO* array and integrated CAG-130 repeats at chromosome six. The *lacO* array is located 6.4 kb away from CAG-130. Adapted from Su et al., 2015. Figure created in part with BioRender.com.

Methods

Strain Construction

All strains, plasmids, and primers mentioned are listed in the supplement. A two-color localization strain containing Nup49-mCherry and CFP-LacI was first made by mating strains 5779 and 2596 (Supplemental Table 1). Colonies that grew on uracil-lacking media and hygromycin-containing media but did not grow on histidine and leucine containing media were selected. Colonies were confirmed to have correct CAG-130 tract length and a good quality focus at the CAG repeat locus. Mating types of each colony was determined, and successful colonies were saved as strains 5800 and 5801 (Supplemental Table 1).

The pRS315-Rad51 plasmid was a generous gift from Jim Haber and the pKT103 plasmid was a generous gift from Kurt Thorn. The Rad51-mVenus plasmid was made by amplifying the Rad51 sequence using the pRS315-Rad51 plasmid as a template and primers 3371 and 3372 that exclude the Rad51 stop codon (Supplemental Tables 2 and 3). The mVenus fragment was amplified using the pKT103 plasmid and primers 3369 and 3370 that contain a GGSGGS amino-acid linker sequence (Supplemental Tables 2 and 3). The resulting PCR products were confirmed to have the correct base pair lengths via gel electrophoresis and remaining PCR products were purified. The fragments were assembled using Gibson assembly and a portion of the reaction mix was transformed into bacteria. The plasmid was then isolated from resulting bacterial colonies through a miniprep. The plasmid was confirmed to have the correct sequence through the Rad51-mVenus portion and had the correct plasmid length and junctions by gel electrophoresis. Bacteria containing the Rad51-mVenus plasmid were stored and saved as plasmid stocks 850 and 851 (Supplemental Table 2).

The wildtype three-color localization strain was made using lithium acetate transformation of the Rad51-mVenus plasmid into strain 5800. Colonies that survived on leucine-lacking plates were

confirmed to have the correct tract length and then saved as strains 5852 and 5853 (Supplemental Table 1). Mutant strains were made by amplifying the resistance marker at the appropriate locus in strains already containing the desired knockout. The resulting PCR product was transformed into strain 5800 and colonies were confirmed to have the correct gene replacement by confirming ORF absence and 5' and 3' junctions. CAG-130 tract lengths were confirmed, and colonies were saved as glycerol stocks. The Rad51-mVenus plasmid was then transformed into mutant strains to yield mutant three-color localization strains, which were also saved as glycerol stocks.

Mating and Random Spore Analysis

Mating was completed by suspending single colonies of each mating type into deionized water and plating on a W303 background-specific sporulation plate. Cells were incubated for five days at 30°C and checked for sporulation with a light microscope.

Random spore analysis was completed by suspending cells in a Zymolyase solution (500 µg/mL Zymolyase-100T and 20 mM 2-Mercaptoethanol in 1.2 M Sorbitol in PBS) and incubated at 30°C for 30 minutes without agitation. Following the addition of 500 µL of water, cells were incubated overnight in a rotator. The following morning, Tween-20 was added to a final concentration of 0.02%, cells were vortexed, then plated onto YEPD plates at a 1:1000 dilution. Resulting single colonies were screened for the desired genotype.

The mating type of each colony was determined using a modified version of the methods described in Arras et al., 2020. The colony in question was picked into two PCR tubes containing YEPD liquid media and combined with either a known mat alpha or mat a strain. Suspensions were vortexed and allowed to rest on the benchtop overnight. Colonies that mate together are visible as they "creep" up the PCR tube (Arras et al., 2020).

PCR to Confirm CAG-130 Tract Length

Prior to experiments, CAG-130 tract lengths were confirmed by PCR and gel electrophoresis. Primers 3107 and 3108 were used to amplify a fragment of DNA containing CAG-130 (Supplemental Table 3). Products of the reaction were visualized on a 2% MetaPhor agarose gel.

Plasmid Construction Tools

PCR products for Gibson assembly were purified using the Zymo Research DNA Clean and Concentrator kit following manufacturer's protocol. The NEBuilder HiFi DNA Assembly kit was used to assemble plasmids following manufacturer's protocol. A two-fold molar excess of vector was used in all assembly reaction mixes. All plasmids were transformed into DH5 alpha cells. The Zymo Research plasmid miniprep kit was used to isolate plasmids from bacteria following manufacturer's protocol.

Lithium Acetate Transformation

Lithium acetate transformation was used to integrate knockout fragments into the desired locus of the genome as well as to insert the Rad51-mVenus plasmid (Gietz & Schiestl, 2007). A single colony of the parent strain was inoculated as an overnight culture and diluted back to an OD of 0.2 the following morning. Cells were rotated at 30°C until they reached an OD of approximately 0.8-1.0 and then pelleted. Cells were suspended in a lithium acetate, Tris-EDTA, and PEG solution along with the knockout fragment or plasmid, and carrier ssDNA. The solution was rotated for 30 minutes at 30°C, followed by the addition of 30 µL of DMSO, and then a 40-minute heat shock at 42°C. A 2-hour liquid recovery in YEPD was used when the knockout fragment contained the kanMX or natMX genes and then cells were plated on G418 or NAT-

containing plates. No liquid recovery was needed when inserting the Rad51-mVenus plasmid since it is selected for using an auxotrophic marker, and cells were plated on leucine-lacking plates.

Long-term Storage of Constructs

Yeast and bacteria were cultured overnight at 30°C or 37°C respectively. Constructs were saved as a glycerol stock containing 1440 µL of the overnight culture and 360 µL of 75% glycerol, and stored at -80°C.

Colocalization Assays

Ibidi 8-well uncoated microscope slides were coated in a 2 mg/mL concanavalin A solution prior to the experiment. Cells were grown overnight at 30°C and diluted back to a 0.2 OD the following morning. Liquid cultures were rotated at 30°C until an OD of approximately 0.5-0.8 was reached. Cells were vortexed vigorously and then aliquoted into each well in sufficient quantity to coat the surface of the slide, typically about 300 µL. To fix cells, paraformaldehyde (PFA) was added to each well at a final concentration of 4% and cells were incubated in the dark for 10 minutes. 4 µL of 3M glycine was added and incubated for 5 minutes to quench fixation. Cells were washed 3 times with 1x phosphate buffered saline (PBS) and then added to coat the surface of each well prior to imaging.

Cells were imaged using the DeltaVision Ultimate Focus 100x lens. Z-scanning was performed to take 26 sections with a 0.20 µm distance between each section. All stacks were analyzed, which is different than the previous literature that only scored the middle two-thirds of nuclear stacks (Whalen et al., 2020). It is also important to note that a Z-stack of 1 or 26 does not necessarily correspond perfectly to the bottom or top of the nucleus, since this depends on if the cell was exactly in focus at the center Z-stack prior to imaging through the planes. This may not always be the case since multiple cells are imaged at once. Thus, it is important to take an

individualized approach when assessing if the Rad51 focus lies within the middle two-thirds of the nucleus or not. However, wildtype cells that were ultimately scored as having a Rad51-mVenus focus colocalized with the CAG repeat focus at the nuclear interior were all confirmed to have their foci located within the middle two-thirds of the nucleus stacks. This ensures that the discrepancy between the wildtype Rad51 loading findings of Whalen et al., 2020 and the results of these experiments were not due to misassigning the location of Rad51 foci. Fluorescence imaging was performed by using the yellow and cyan channels at a 200-millisecond exposure time per Z-plane and a 10% transmission, and the red channel at a 0.5 second exposure time and 10% transmission. The polarized light setting was at a 0.1 second exposure time and 10% transmission. The order in which cells were exposed to the four channels was yellow, cyan, red, and lastly polarized light. Images were deconvolved to improve contrast and resolution.

Only cells in late S phase were scored, which was determined by round nuclei and a bud size proportion between 0.2 and 0.5 (Bud size during S phase data collected by Jenna Whalen, not shown). Bud size proportions for each cell was measured using ImageJ by fitting an ellipse to the bud and mother cell, measuring the area, and dividing the bud size area by the mother cell area. Only cells containing at minimum one Rad51 focus per nucleus were scored, following the methods of Whalen et al., 2020. The Z-projection function of ImageJ was used to assist in characterizing foci. Brightness and contrast settings were also optimized for each image to better visualize foci. To determine where the CAG repeat locus is within the nucleus, two distances were calculated. First, the distance between the CFP-LacI/LacO focus and the middle of the nearest nuclear pore was measured. Then, the diameter of the nucleus was measured and halved to render the radius. The proportion between these two measurements was used to characterize the location of the CAG repeat locus into three distinct zones: zone 1, zone 2, and zone 3. A zone measurement

of less than 0.184 corresponds to zone 1 and zone measurements greater than 0.422 correspond to zone 3 (Meister et al., 2010). Zone 1 indicates that the CAG repeat locus is at the nuclear pores, whereas in zones 2 and 3 it is not at the nuclear pores (Figure 9).

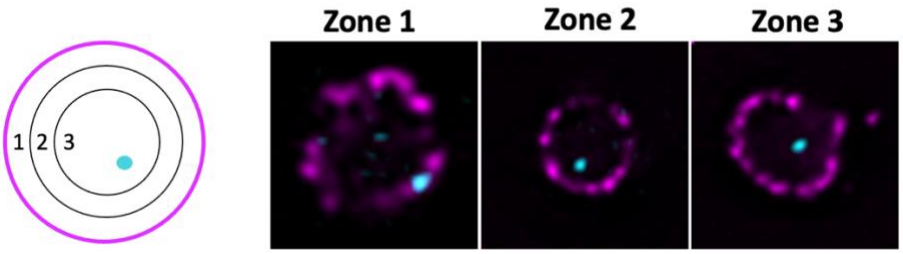

Figure 9. Model of the zones within the nucleus, adapted from Su et al., 2015. Examples images of CAG repeat locus situated in each zone when the repeat locus is marked with CFP-LacI/*lacO* and the nuclear pores with Nup49-mCherry.

To determine the colocalization status of the Rad51 focus and the CFP-LacI/*lacO* focus, the distance between the brightest points of each focus was measured. If the foci were located within the same Z plane, only one measurement directly from the brightest points of each focus was necessary to measure the distance. However, if the foci were in differing Z planes, a slightly different approach was taken to account for the distance in the Z-plane in addition to X and Y planes (Figure 10). First, the distance between the Rad51-mVenus focus and CFP-LacI/*lacO* focus was measured using a 2-D projection. A 2-D projection, or Z-projection, places the brightest points of each focus into the same plane, making it possible to measure the distance between foci that otherwise would be in different planes. Then, the number of Z-planes was determined between the foci and multiplied by 0.2 µm to give the corresponding Z-distance. The Pythagorean theorem was used to determine the hypotenuse of the resulting triangle, which corresponds to the true distance between the Rad51 focus and the CFP-LacI/*lacO* focus (Figure 10).

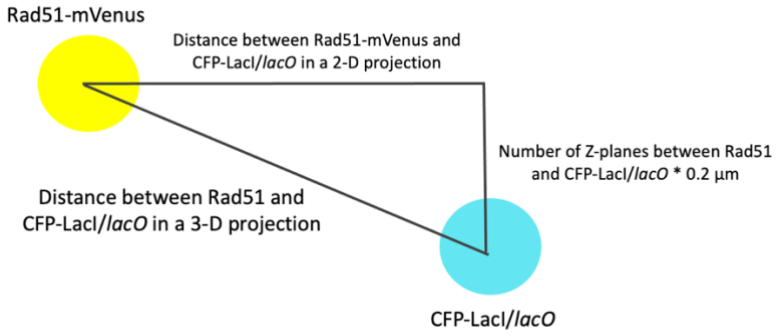

Figure 10. Measuring the distance between a Rad51-mVenus focus and a CFP-LacI/*lacO* focus that are in different Z-planes using the Pythagorean theorem.

Results

Determining a Colocalization Threshold

To properly characterize colocalization of foci, it is important to consider how elements that form foci visually appear under the microscope and the corresponding distance between the foci. To this extent, since the *lacO* array is positioned 6.4 kilobases away from the CAG-130 repeats we assessed how structures that are a certain distance away from each other in the genome visually appear when imaged with the DeltaVision Ultimate Focus fluorescent microscope used in this study. Previously, using the Zeiss AX10 fluorescent microscope, these elements were reported as spatially indistinguishable under 100x magnification (Su et al., 2015). However, with the higher spatial resolution offered with the DeltaVision microscope, it became necessary to confirm that these elements remain indistinguishable. If elements are completely overlapped or have a 0 μm distance between the two foci, it is safe to assume that the proteins are colocalized. If these are not microscopically indistinguishable, this would mean that there is a certain distance at which the repeat locus could be colocalized with Rad51, but the Rad51 and *lacO* array foci themselves would not be overlapped. We therefore sought to determine if the CAG repeat locus and the *lacO* array are indistinguishable when imaged using the DeltaVision microscope. To do so, we conducted an experiment with a strain that contains a *lacO* array and a *tetO* array that are 26.6 kilobases away from each other (Supplemental Table 1). The arrays in this strain contain 128 copies of the *lacO* or *tetO* sequence respectively, different than the 256 copies of the *lacO* sequence in the strains used in the colocalization assays. A strain with two fluorescently tagged loci 6.4 kilobases away from each other with 256 copies of the arrays was not currently available, so this was the next best option. By quantifying the average distances between the two foci, we can determine whether the potential upper limit of 26.6 kilobases is spatially indistinguishable using the DeltaVision microscope.

The results of this experiment suggest that the average distance between these two elements was 0.183 µm which would correspond to the two foci being adjacent to each other (touching) in most cells (Figure 11B, Figure 12). However, there was variability in these measurements since the foci distances ranged from 0 µm to 0.462 µm, which corresponds to foci being partially overlapped or separated (Figure 11A, Figure 11C, Figure 12). Therefore, most foci were distinguishable visually, meaning adjacent (touching) or entirely separated. Additionally, there were discrepancies between the qualitative visual appearance of the foci and the quantitative distance measurements. For example, Figure 11B shows the foci to be adjacent (touching) at 0.196 µm, but foci could also appear to be adjacent (touching) at a maximum distance of 0.3 µm. Taking all this together, a colocalization threshold of 0.3 µm was used to determine whether the Rad51-mVenus focus was colocalized with the CFP-LacI/*lacO* focus (see Discussion for further justification). Foci that were less than a 0.3 µm away from each other were considered colocalized.

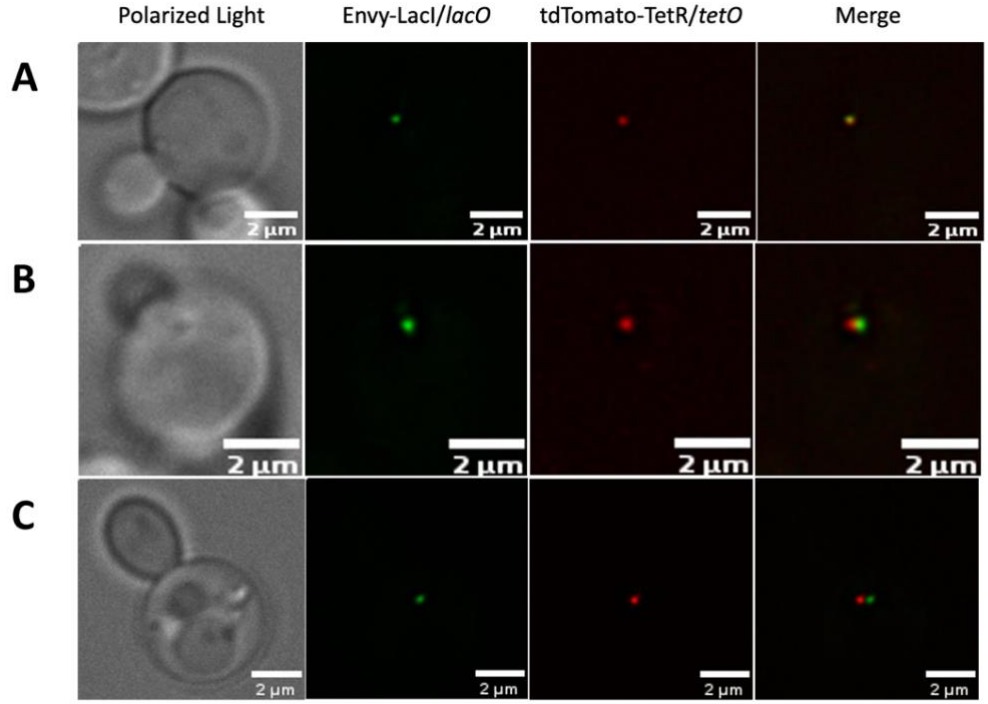

Figure 11: Representative microscopy images depicting the Envy-LacI/*lacO* and tdTomato-TetR/*tetO* foci that are situated 26,585 kilobases away from each other in the genome. (A) The two foci are visually partially overlapped at 0 µm. (B) The two foci are adjacent (touching) at 0.196 µm. (C) The two foci are entirely separated at 0.429 µm.

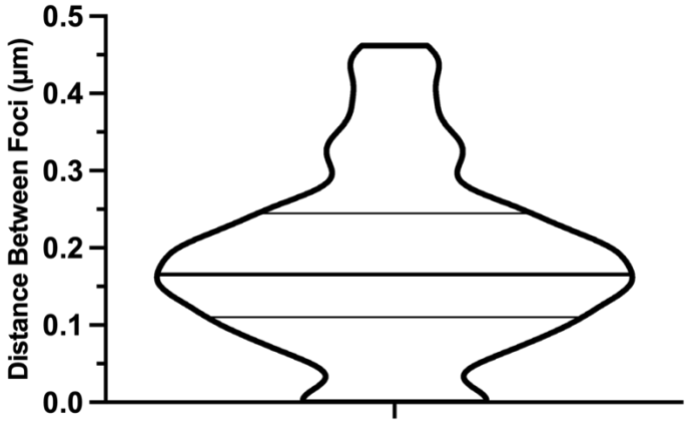

Figure 12. Distance Between Envy-LacI/*lacO* and tdTomato-TetR/*tetO* foci (µm). These arrays are 26.6 kb away from each other within the genome, a *lacO*x128 non-repetitive array at chrIV:332,960, and *tetO*x128 non-repetitive array at chrIV:352,560. Median value is 0.166, first quartile is 0.111, and third quartile is 0.244. Mean distance is 0.183 µm and one standard deviation is 0.112 µm (not shown on graph). n=82 cells.

Rad51 Colocalization with CAG Repeat Locus is Dependent on Slx8

To understand which proteins might affect Rad51 loading at the CAG repeats, we developed a three-color strain that tags the nuclear pore protein Nup49 with mCherry, tags Rad51 with mVenus on a plasmid, and uses the CFP-LacI/*lacO* system to locate the repeat locus (Figure 13). To assess whether the Slx8, Srs2, or Sgs1 proteins are involved in Rad51 loading before or after CAG repeat relocation to the NPC, *slx8*, *srs2*, and *sgs1* knockout strains were created in the three-color strain background. For each cell scored, the bud sizes, distance from the CFP-LacI/*lacO* focus to the NPC, distance between the brightest points of the Rad51-mVenus and CFP-LacI/*lacO* foci, and diameter of the nucleus was measured (see Methods). The Rad51-mVenus and CFP-LacI/lacO foci were considered colocalized if the distance between the brightest points of the foci was less than or equal to 0.3 µm. From these measurements, the zone measurement and

colocalization status was determined and plotted using a scatterplot (Figure 14). The percent colocalization was determined in each strain when the repeat was at the NPC or not at the NPC (Figure 15). The Fischer's exact test was used to determine significance as compared to the respective wildtype value. This statistical test was chosen since a contingency table can be created using the number of cells containing colocalized foci at the NPC or not at the NPC. By comparing the wildtype strain counts with the mutant strain counts, the Fischer's exact test can determine if these frequencies demonstrate a statistically significant difference.

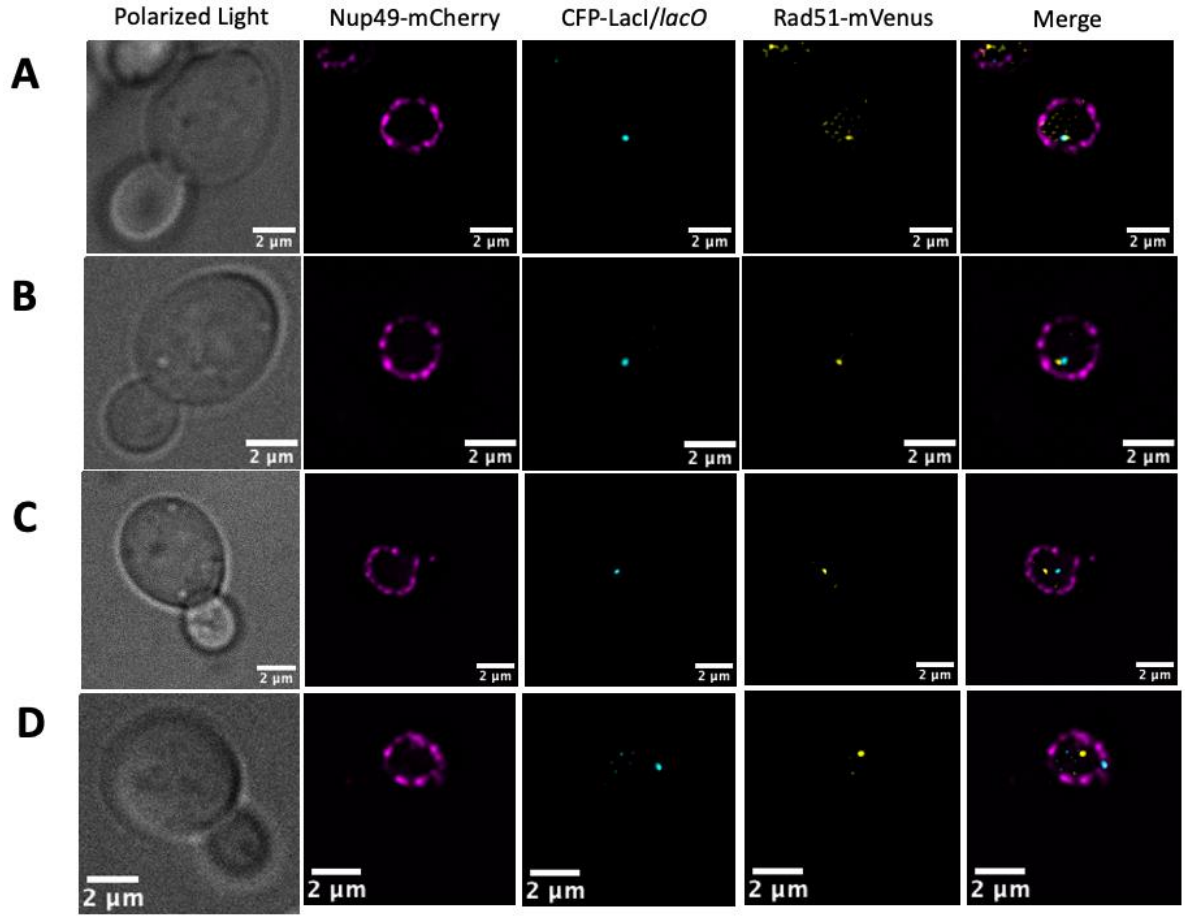

Figure 13. Representative microscopy images using three-color strain. (A) Zone 1, foci are colocalized. Bud size = 0.497, zone measurement = 0.121 µm, distance between Rad51-mVenus and CFP-LacI/*lacO* = 0 µm. (B) Zone 3, foci are colocalized. Bud size = 0.283, zone measurement = 0.495 µm, distance between Rad51-mVenus and CFP-LacI/*lacO* = 0.168 µm. (C) Zone 3, foci are not colocalized. Bud size = 0.240, zone measurement = 0.715 µm, distance between Rad51-mVenus and CFP-LacI/*lacO* = 0.628 µm. (D) Zone 1, foci are not colocalized. Bud size = 0.270, zone measurement = 0 µm, distance between Rad51-mVenus and CFP-LacI/*lacO* = 1.395 µm.

The results of the wildtype data suggest that before the repeats relocate to the NPC, Rad51 colocalizes with the CAG repeat locus 19.5% of the time (Figure 14A, Figure 15). After relocation, Rad51 colocalized with the CAG repeat locus in 17.4% of cells counted (Figure 14A, Figure 15). In the wildtype cells, there was no statistical difference in Rad51 loading prior to or after relocation of the CAG repeats to the NPC using Fischer's exact test, since the test statistic was 1 (not shown). Therefore, these data suggest that there is no difference in Rad51 loading based on where the repeat is in relation to the NPC in wildtype cells, which is inconsistent with the findings of Whalen et al., 2020.

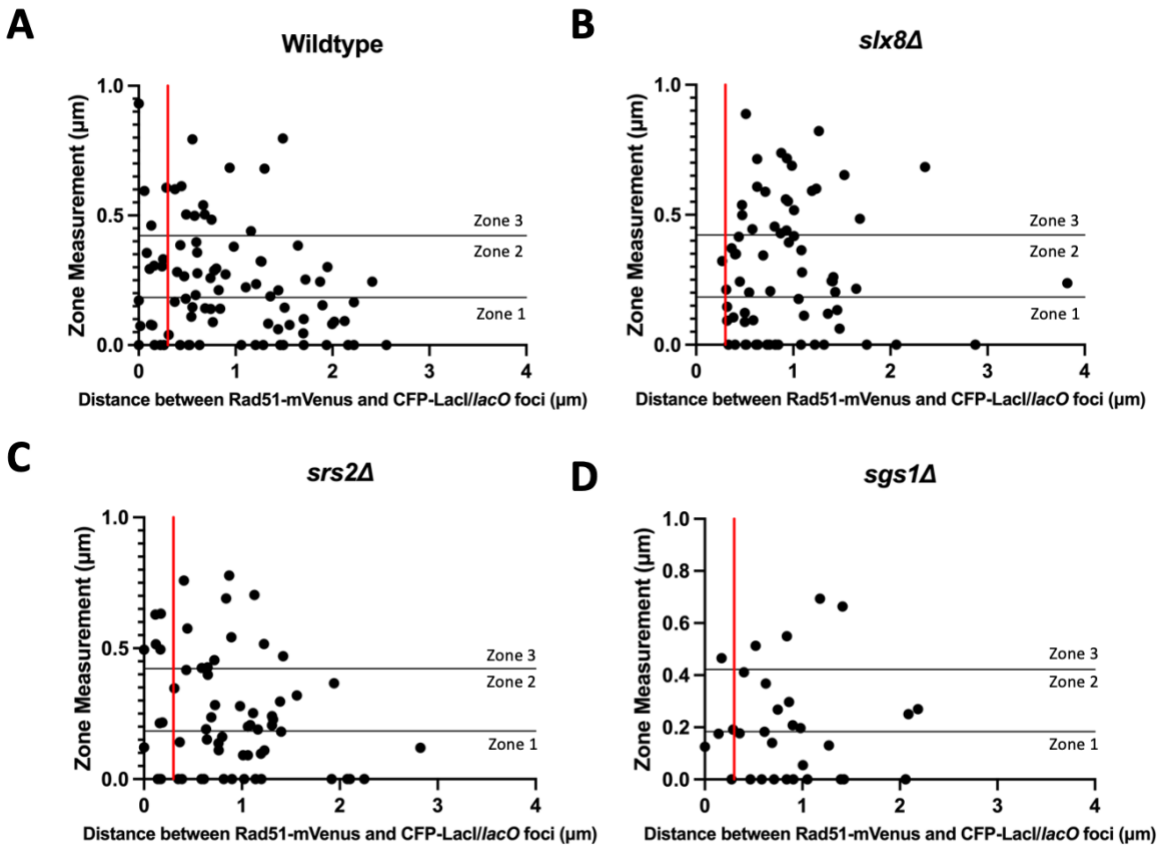

Figure 14. Scatterplots depicting relationship between colocalization status and zone measurement. Colocalization status determined using a threshold of 0.3 µm distance between the Rad51-mVenus and CFP-LacI/*lacO* foci (vertical red line). Zone measurement is determined by dividing the distance from the repeat locus to the NPC by the radius of the nucleus. Zone measurements between 0 µm and 0.184 µm are zone 1, between 0.184 µm and 0.422 µm are zone 2, and measurements greater than 0.422 are zone 3. Zone

1 indicates the CAG repeat locus is at the NPC whereas zones 2 and 3 indicate it is not at the NPC. (A) Wildtype cells, n=87. (B) *slx8*Δ cells, n=71. (C) *srs2*Δ cells, n=63. (D) *sgs1*Δ cells, n=31.

A

Strain Type	% Rad51 Foci Colocalized with CAG Repeat Locus at the NPC	% Rad51 Foci Colocalized with CAG Repeat Locus Not at the NPC
Wildtype	19.5%	17.4%
slx8Δ	0.00%*	2.17%*
srs2Δ	12.0%	20.0%
sgs1Δ	21.4%	7.69%

B

Mutant Strain	Fischer's Exact Test Statistic for % Rad51 Foci Colocalized with CAG Repeat Locus at the NPC compared to WT	Fischer's Exact Test Statistic for% Rad51 Foci Colocalized with CAG Repeat Locus Not at the NPC compared to WT
slx8Δ	0.0203	0.0302
srs2Δ	0.5053	0.7804
sgs1Δ	1.0000	0.6705

C

Strain Type	Number of Rad51 Foci Colocalized with CAG Repeat Locus at the NPC	Number of Rad51 Foci Not Colocalized with CAG Repeat Locus at the NPC	Number of Rad51 Foci Colocalized with CAG Repeat Locus Not at the NPC	Number of Rad51 Foci Not Colocalized with CAG locus Not at the NPC	Total Number of Cells Counted
Wildtype	8	33	8	38	87
slx8Δ	0	25	1	45	71
srs2Δ	3	25	7	28	63
sgs1Δ	3	14	1	13	31

Figure 15. (A) Percent colocalization of Rad51-mVenus with CFP-LacI/*lacO* in each strain type based on relationship to the NPC. Only cells with Rad51 foci were counted. Zone 1 corresponds to the repeats being located at the NPC, whereas zones 2 and 3 indicate the repeats are not at the NPC. * Indicates significantly different than the corresponding wildtype percentage. (B) Fischer's exact test was performed to determine significance using a significance level of 0.05. Test statistic for the *slx8*Δ data was 0.0203 when the repeats are at the NPC and 0.0302 when the repeats are not at the NPC. These data were deemed statistically significant. All *srs2*Δ and *sgs1*Δ data resulted in test statistics greater than 0.05 and therefore were not significantly different than their corresponding wildtype data. (C) Number of cells counted for each condition and total counts (n values).

In the *slx8*Δ cells, Rad51 was never observed to be colocalized with the CAG repeat locus prior to relocation to the NPC (Figure 14B, Figure 15A). The 0.00% colocalization of Rad51 with the CAG repeat locus prior to relocation to the NPC was significantly different than the 19.5% colocalization observed in wildtype cells (Figure 15B). Additionally, the 2.17% colocalization of Rad51 with the CAG repeat locus after relocation was significantly different than the 17.4% observed in wildtype cells (Figure 15). Since colocalization of Rad51 is significantly decreased when Slx8 is absent from cells, this suggests that Slx8 is needed to facilitate Rad51 loading before and after relocation of the repeats to the NPC.

In *srs2*Δ and *sgs1*Δ cells, no statistical differences in Rad51 loading were observed in either mutant compared to wildtype cells, regardless of location of the repeats in relation to the NPC (Figure 15). Since the absence of the Srs2 and Sgs1 proteins from the cell do not affect Rad51 colocalization with the CAG repeat locus, this suggests that these proteins are not directly involved in facilitating Rad51 loading at the repeat tract. However, it is important to note that the n value for the *srs2*Δ experiment was 63 and *sgs1*Δ was 31. Therefore, there is stronger support for the idea that Srs2 is not needed for Rad51 loading as opposed to Sgs1, but more cells should be counted in future experiments.

Discussion

Justifying a Colocalization Threshold

In most instances, the 26.6 kilobase rendered foci to appear touching or partially overlapped, making this distance visually distinguishable. The average distance between the foci was 0.183 µm which corresponds best to the foci touching each other (Figure 11B, Figure 12). There were instances where the foci were a 0 µm distance from each other but visually appeared to be partially overlapped (Figure 11A). At the upper end, there were few instances where the foci were entirely not touching, which occurred at around 0.4 µm (Figure 11C). Visually, it would appear as though it is possible to spatially distinguish between two structures that are 26.6 kilobases away, as for most foci would be either partially overlapped, touching, or entirely separated. In our strains, the *lacO* array is 6.4 kilobases away from the CAG repeats. It is most likely the case that elements that are 6.4 kilobases away would range from visually touching or entirely overlapping, but not separated. It is likely not the case that if the Rad51-mVenus focus and CFP-LacI/*lacO* foci are entirely separated visually that there is still colocalization between the two elements.

The upper limit of foci that are touching corresponded to an approximately 0.3 µm distance and this was used as the colocalization threshold. This is in line with previous experiments where foci that are touching were considered colocalized (Whalen et al., 2020). In our strains, it is possible that when the Rad51-mVenus focus is touching the CFP-LacI/*lacO* focus that there is true colocalization of Rad51 with the CAG repeats and therefore these cells were included in colocalization measurements. However, foci that are not touching at all are unlikely to have true colocalization of Rad51 with the repeats, and therefore cells that showed a greater than 0.3 µm distance between the foci were considered not colocalized.

Implications of this Study

In the above experiments, we used the CAG-130 structure-forming repeats to study proteins involved in Rad51 loading at the tract before and after relocation to the NPC. Previous research had suggested that Rad51 loading occurs while the repeats are at the NPC and that Rad51 is excluded prior to relocation in a manner dependent on RPA-SUMO (Whalen et al., 2020). The results of this experiment found that Rad51 association at the repeat locus was not significantly different between the repeat locus being not at the NPC and the repeat locus being at the NPC, contradicting earlier findings. This discrepancy can best be attributed to several key experimental differences. Prior studies had used the Zeiss AX10 fluorescent microscope with the 100x lens whereas this study uses the DeltaVision Ultimate Focus with the 100x lens. The images rendered from each of the microscopes have stark differences, particularly since the DeltaVision microscope can capture images with a higher resolution than the Zeiss microscope, which may allow for detection of smaller or dimmer Rad51 foci that possibly would not have been previously observed (compare Figure 4B with Figure 13). Additionally, the strains used in the experiments in this study mark each structure with its own fluorescent marker. This allows for easier and more reliable identification of structures and their location within the nucleus. Lastly, this experiment uses a different means of quantifying colocalization. Previous experiments had considered spatial overlap of foci to be colocalization, but this experiment uses a novel approach to assess colocalization by measuring distances between the foci and binning colocalization instances using a predetermined threshold.

It is important to reiterate that the strains used in this experiment contain the wildtype RAD51 at the chromosomal locus and a RAD51-mVenus separated with the GGSGGS amino-acid linker on a CEN plasmid (Supplemental Tables 1 and 2). Centromeric plasmids can exist in 2-4

copies in *Saccharomyces cerevisiae* cells (Karim et al., 2013). Therefore, it is possible that the tagged Rad51-mVenus is in greater abundance within the cell than untagged Rad51. Previously, the RAD51-GFP fusion protein has been shown to locate normally to sites of DNA damage but is unable to catalyze homologous recombination (Da Ines et al., 2013). Further, in yeast it has been shown that this mutation is not dominant negative, and as long as the tagged RAD51 is complemented with an untagged wildtype RAD51, Rad51 foci can form and repair by recombination can still occur (Waterman et al., 2019). In this study, we have not yet explicitly shown that the strains we used are not acting as dominant negative. To address this, an MMS sensitivity assay was performed (Supplemental Figure 13). Given that mVenus (Kremers et al., 2006) is a close derivative of GFP (Prasher et al., 1992), we predicted it would be unlikely that this would drastically affect Rad51 activity. In fact, the GFP sequence and mVenus sequences are 94.61% similar, with 11 amino acid substitutions and 1 amino acid insertion (alignment between amino acid sequences not shown). The results of this experiment showed some MMS sensitivity in one wildtype strain (Supplemental Figure 13). This experiment should be repeated with both wildtype strains to further substantiate these results.

To assess which proteins are involved in facilitating the loading of Rad51 at the repeat locus, we created mutant strains that knocked out key proteins of interest and assessed the impact on colocalization of Rad51 with the repeat locus. The results of these experiments would suggest that Slx8 is involved in facilitating Rad51 loading both before and after relocation of the repeats to the NPC. In part, this data is consistent with previous findings that Rfa1 is present is slightly decreased quantities when the repeats are at the NPC compared to before relocation (Whalen et al., 2020). This somewhat supports our hypothesis that Slx8 may target RPA-SUMO for degradation after relocation to the NPC, rendering a single-stranded platform to which Rad51 can

bind. However, this does not completely explain how Slx8 might be facilitating Rad51 loading even before the repeat locus relocates to the NPC. Previous research has found Rad52 to be a target of SUMOylation that was targeted for degradation by the Slx5-Slx8 complex (Su et al., 2015). In line with this, it is reasonable that in the absence of Slx8, ubiquitylation of Rad52-SUMO is not occurring and consequently Rad52-SUMO is not degraded. Rad52-SUMO has been shown to have a decreased ability to promote Rad51 filamentation (Esta et al., 2013). This would explain the global decrease in Rad51 colocalization with the repeat locus before and after relocation to the NPC, since Rad52-SUMO accumulation would decrease Rad51 filamentation regardless of where the repeat locus is positioned.

There are several ways to test the reasoning that Rad52-SUMO levels are increased in the absence of Slx8, and that this is responsible for the global decreases in Rad51 loading. The major SUMOylation sites of Rad52 have been previously characterized as K10, K11 and K220 (Sacher et al., 2006). Introducing point mutations at one or more of these sites by changing the SUMOylatable lysine residue to a non-SUMOylatable arginine residue will drastically decrease levels of Rad52 SUMOylation. Previous research has characterized only the *rad52-3KR rad59-2KR* double mutant (Whalen et al., 2020). In the single mutant, containing *rad52*^{K10,11,220R}, we would expect to see increased Rad51 loading compared to wildtype, since the abundance of Rad52 present, but not Rad52-SUMO, would facilitate much more Rad51 loading. In the double mutant, containing *slx8*Δ and rad*52*^{K10,11,220R}, we would expect to see Rad51 loading restored to wildtype levels. This is because Rad51 loading is decreased in the absence of Slx8, but if Rad52 were not SUMOylated, then Slx8 being absent would not impact degradation of Rad52-SUMO, and Rad52 would facilitate loading of Rad51 at a frequency similar to wildtype values. In these experiments, Rad51 loading could be measured using a colocalization fluorescence assay.

Another possible explanation for the global decrease in Rad51 loading is that Slx8 serves to negatively regulate Rad52-dependent recombination events (Burgess et al., 2007). Previous findings have shown that in the absence of Slx8, the SUMOylation levels of RPA, Rad52, and Rad59 decreased, with Rad52 SUMOylation being the least affected of the three proteins (Burgess et al., 2007). It has also been shown that Rad52-dependent recombination events increase and Rad52 foci increase when Slx8 is absent from the cell (Burgess et al., 2007). These findings suggested that SUMOylation by Slx8 regulates Rad52-dependent recombination, and therefore, it is possible that in the absence of Slx8, Rad52-mediated recombination events that occur during SSA and BIR pathways are no longer disfavored. This would explain why Rad51 is not observed at the repeats, as Rad51 is not required for SSA (Bhargava et al., 2016), and is not needed in Rad51-independent BIR (Malkova et al., 1996). It would be interesting to see whether in the absence of Slx8 we would observe increased SSA or BIR repair processes.

The results of this experiment begin to suggest that Srs2 and Sgs1 are not directly involved in facilitating Rad51 loading. If Sgs1 or Srs2 were disrupting Rad51 filaments prior to the repeats relocating to the NPC, we would have expected to see increased Rad51 association with the CAG repeat locus in the absence of these proteins. Instead, we saw no statistically significant difference in colocalization of Rad51 with the repeat locus in the absence of Srs2 or Sgs1 (Figure 15A). It is important to clarify that the results of the Whalen et al., 2020 did not show a difference in CAG repeat relocation to the NPC when independently removing Sgs1 or Exo1 but did find a significant decrease in relocation when both were removed. Thus, in the *sgs1*Δ mutant experiment, we predominantly sought to test the role of its helicase activity, since resection would still occur via Exo1. The results of this experiment begin to suggest that Srs2 and Sgs1 may not be recruited by RPA-SUMO prior to relocation to facilitate Rad51 loading. However, it is necessary to proceed

with caution as the n-value in these experiments were low. If it truly is the case that neither Srs2 nor Sgs1 are recruited to the replication fork before relocation, they may not be targeted for degradation at the pores to facilitate Rad51 loading.

Additional Future Directions

While adding a quantitative element is superior to the descriptive method of subjectively noting visual differences between foci to determine colocalization, it is certainly not without its flaws. The method of quantifying distances between foci which was used in these experiments necessitates determining an accurate and reliable colocalization threshold. Although the *tetO*/*lacO* experiment used in this study is certainly a start, additional experiments to determine the most reasonable colocalization threshold should be performed. The most ideal experiment would be to place a *tetO* and *lacO* array 6.4 kilobases away from each other and determine the distance between the two foci. This can be done using a strain that already contains the *lacO* array and no CAG repeats, then insert a *tetO* array at the CAG repeat locus. This would provide more confidence that a threshold of 0.3 μm is the most appropriate choice to assess colocalization. Additionally, this would provide visual confirmation that a 6.4 kilobase genomic distance is truly spatially indistinguishable using the DeltaVision microscope.

It is important to note first, that the visual spatial difference did not always correlate well with the quantitative distance. For example, sometimes foci that are 0.2 μm apart appear to be completely separated. Additionally, foci that are 0 μm apart could either be either entirely overlapped or partially overlapped. A potential experiment that could be performed to resolve this discrepancy is to quantify the percentage of overlap between the foci and correlate these values to the distances between the brightest points of the focus. One benefit from such an experiment would be that it can tie together the visual aspect of fluorescence microscopy with the quantitative aspect.

An additional benefit is that using percentage overlap of the foci in addition to distances between the brightest points of each focus would provide a further means of support when determining a distance colocalization threshold.

The colocalization assays of this study should be repeated to increase the cell counts for each condition. A minimum of 100 cells in each strain should be counted, but more confidence in the results could be established with cell counts of 150 or greater. Additional experiments should be performed to supplement the colocalization assay and confirm how the Slx8 protein impacts Rad51 loading in differing experimental contexts. An alternative means to address this is through a proximity ligation assay (PLA). This experiment would incorporate the thymidine analogue BrdU during S phase to characterize newly synthesized DNA at the repeat. A large fluorescent signal would be generated if the Rad51 protein comes within proximity of the newly synthesized DNA at the repeat locus. Another interesting experiment to conduct would be chromatin immunoprecipitation (ChIP). Using an antibody against the Rad51 protein, it would be possible to extract the regions of DNA that Rad51 binds and ultimately determine the frequency at which Rad51 is binding at the repeat locus. These would be effective means to characterize colocalization of Rad51 at the repeats in wildtype cells, and when used within an *slx8*Δ background, to further establish how Slx8 impacts Rad51 loading at the repeat locus. An additional concept that would also be interesting to test is the Rad51 loading in a *rad59*Δ single mutant strain. There is evidence to support that Rad59 associates with Rad52 in a ring-like structure (Davis, 2003). Increased Rad59 presence within the ring, in the absence of Rad52, may decrease overall recruitment of Rad51 at CAG repeats compared to a wildtype background.

Supplement

Supplemental Table 1. Yeast Strains

Strain Number	Strain Background	Genotype	Description	Citation
2596	W303	MATa, nup49::NUP49-GFP ARS607-LacOR-TRP1 his::GFP-LacI:HIS ura3-1 leu2-3, 112257 trp1-1 ade2-1 can1-100	Mating strain to make two-color localization strain 5800 and 5801	(Su et al., 2015)
3833	YMV80	srs2::KanMX6, MAT::hisG, hml::ADE1 hmr::ADE1, ade1, lys5, ura3-52, trp1, ade3::GAL-HO, leu2::cs, CTG-70	Used to amplify kanMX at srs2 locus to create strains 5896 and 5897.	Made by Erica Polleys
5027	yPH499	sgs1::KanMX6, MATa, ura3-52, trp1-Δ63, his3-Δ200, leu2-Δ1; ade2Δ::hisG (salmonella), LYS2::ADE2::URA3-F1	Used to amplify kanMX at sgs1 locus to create strains 5889 and 5890.	Made by Jaylee Boer
5545	W303	slx8::NATMX, rfa1-smt3dGG-KANMX, GFP-Nup49; GFP-LacI/LacO-CAG-130	Used to amplify natMX at slx8 locus to create strains 5894 and 5895.	This study
5779	W303	MATalpha, nup49::NUP49-mCherry ARS607-LacOR-TRP1, ura3-1::HIS3p-CFP-LacI-URA3, leu2-3, 112 trp1-1, ade2-1 can1-100; CAG-130;Chr6int::lacop-lexAop-TRP1 (Chr6int is 272 bp upstream ARS607) Chr6int2::CAG130 (Chr6int2 is 7645 bp from Chr6int and 560 bp upstream of tA(AGC)F) TUB1-mVenus-Tub1:LEU2	Mating strain to make two-color localization strain 5800 and 5801	Made by Tyler Maclay and Anicka AbiChedid
5800, 5801	W303	MATa, nup49::NUP49-mCherry, ARS607-LacOR-TRP1, ura3-1::HIS3p-CFP-LacI-URA3, leu2-3, trp1-1, ade2-1 can1-100; Chr6int::lacop-lexAop-TRP1 (Chr6int is 272 bp upstream ARS607) Chr6int2::CAG130 (Chr6int2 is 7645 bp from Chr6int and 560 bp upstream of tA(AGC)F)	Two-color localization strain that marks the repeat locus with CFP and Nup49 with mCherry. Contains CAG-130.	This study
5852, 5853	W303	MATa, nup49::NUP49-mCherry, ARS607-LacOR-TRP1, ura3-1::HIS3p-CFP-LacI-URA3, leu2-3, trp1-1, ade2-1 can1-100; Chr6int::lacop-lexAop-TRP1 (Chr6int is 272 bp upstream ARS607) Chr6int2::CAG130 (Chr6int2 is 7645 bp from Chr6int and 560 bp upstream of tA(AGC)F), contains Rad51-mVenus plasmid (#850)	Strains used in wildtype colocalization assay. Marks the repeat locus with CFP and Nup49 with mCherry. Contains a Rad51-mVenus plasmid. Contains CAG-130.	This study
5889, 5890	W303	sgs1::kanMX, MATa, nup49::NUP49-mCherry, ARS607-LacOR-TRP1, ura3-1::HIS3p-CFP-LacI-URA3, leu2-3, trp1-1, ade2-1 can1-100; Chr6int::lacop-lexAop-TRP1 (Chr6int is 272 bp upstream ARS607) Chr6int2::CAG130 (Chr6int2 is 7645 bp from Chr6int and 560 bp upstream of tA(AGC)F)	Sgs1Δ in two-color localization strain background. Marks the repeat locus with CFP and Nup49 with mCherry. Contains CAG-130.	This study
5894, 5895	W303	slx8::natMX, MATa, nup49::NUP49-mCherry, ARS607-LacOR-TRP1, ura3-1::HIS3p-CFP-LacI-URA3, leu2-3, trp1-1, ade2-1 can1-100; Chr6int::lacop-lexAop-TRP1 (Chr6int is 272 bp upstream ARS607) Chr6int2::CAG130 (Chr6int2	Slx8Δ in two-color localization strain background. Marks the repeat locus with CFP and Nup49 with	This study

		is 7645 bp from Chr6int and 560 bp upstream of tA(AGC)F)	mCherry. Contains CAG-130.	
5896, 5897	W303	srs2::kanMX, MATa, nup49::NUP49-mCherry, ARS607-LacOR-TRP1, ura3-1::HIS3p-CFP-LacI-URA3, leu2-3, trp1-1, ade2-1 can1-100; Chr6int::lacop-lexAop-TRP1 (Chr6int is 272 bp upstream ARS607) Chr6int2::CAG130 (Chr6int2 is 7645 bp from Chr6int and 560 bp upstream of tA(AGC)F)	Srs2Δ in two-color localization strain background. Marks the repeat locus with CFP and Nup49 with mCherry. Contains CAG-130.	This study
5903, 5904	W303	slx8::natMX, MATa, nup49::NUP49-mCherry, ARS607-LacOR-TRP1, ura3-1::HIS3p-CFP-LacI-URA3, leu2-3, trp1-1, ade2-1 can1-100; Chr6int::lacop-lexAop-TRP1 (Chr6int is 272 bp upstream ARS607) Chr6int2::CAG130 (Chr6int2 is 7645 bp from Chr6int and 560 bp upstream of tA(AGC)F), contains Rad51-mVenus plasmid (#850)	Strains used in slx8Δ colocalization assays. Marks the repeat locus with CFP and Nup49 with mCherry. Contains a Rad51-mVenus plasmid. Contains CAG-130.	This study
5905, 5906	W303	sgs1::kanMX, MATa, nup49::NUP49-mCherry, ARS607-LacOR-TRP1, ura3-1::HIS3p-CFP-LacI-URA3, leu2-3, trp1-1, ade2-1 can1-100; Chr6int::lacop-lexAop-TRP1 (Chr6int is 272 bp upstream ARS607) Chr6int2::CAG130 (Chr6int2 is 7645 bp from Chr6int and 560 bp upstream of tA(AGC)F), contains Rad51-mVenus plasmid (#850)	Strains used in sgs1Δ colocalization assays. Marks the repeat locus with CFP and Nup49 with mCherry. Contains a Rad51-mVenus plasmid. Contains CAG-130.	This study
5915, 5916	W303	srs2::kanMX, MATa, nup49::NUP49-mCherry, ARS607-LacOR-TRP1, ura3-1::HIS3p-CFP-LacI-URA3, leu2-3, trp1-1, ade2-1 can1-100; Chr6int::lacop-lexAop-TRP1 (Chr6int is 272 bp upstream ARS607) Chr6int2::CAG130 (Chr6int2 is 7645 bp from Chr6int and 560 bp upstream of tA(AGC)F), contains Rad51-mVenus plasmid (#850)	Strains used in srs2Δ colocalization assays. Marks the repeat locus with CFP and Nup49 with mCherry. Contains a Rad51-mVenus plasmid. Contains CAG-130.	This study
S. Mirkin Lab 1205	W1588	MATa leu2-3,112 trp1-1 can1-100 ura3-1 ade2-1 his3-11,15, lacOx128 non-repetitive array at chrIV:332,960, tetOx128 non-repetitive array at chrIV:352,560, pDDlacI-tetR1 at the ADE1 locus (with KAN marker, NAT cassette at chrIV:336,187)	Strain used to measure distance between *lacO* and *tetO* arrays.	S. Mirkin Lab

Supplemental Table 2. Plasmids

Plasmid Number	Plasmid Name	Description	Citation
693	pRS315-Rad51 (WT Rad51 LEU2 CEN)	Contains WT Rad51 under its own promoter and leucine marker. Amplified as vector backbone to create plasmids 850 and 851.	A generous gift from the Haber laboratory.
836	pKT103 (pFA6a–link–yEVenus–Kan)	Amplified mVenus fragment as insert to create plasmids 850 and 851. Addgene #8718	(Sheff & Thorn, 2004)

850, 851	pRS315 LEU2-CEN plasmid with Rad51-mVenus	Tagged WT Rad51 on plasmid 693 with mVenus fragment amplified from plasmid 836. Sequence verified through Rad51-mVenus region, correct Rad51 and mVenus sequences, correct linker (GGSGGS), excludes Rad51 stop codon. Plasmid contains leucine selectable marker. Bacterial colonies 3 and 8.	This study

Supplemental Table 3. Primers

Primer Number	Primer Name	Primer Sequence (5' to 3')	Description
760	Slx8-ChkRev	cgctttgccgagaattgaag	Forward primer to confirm 5' junction in slx8::natMX.
768	slx8 KO for	cagggaaagaaagaactgtttt	Forward primer to amplify natMX at slx8 locus in strain 5545 to create strains 5894 and 5895. Additionally used to check presence of natMX following transformation.
769	slx8 KO rev	ttcctcggagtgctttgttt	Reverse primer to amplify natMX at slx8 locus in strain 5545 to create strains 5894 and 5895. Used to check presence of natMX following transformation. Used as reverse primer to confirm 3' junction in slx8::natMX.
1396	kanMXrev118bpstart	gatagattgtcgcacctgattgcc	Reverse primer to confirm 5' junction in srs2::kanMX and sgs1::kanMX.
1564	Srs2upstreamfor_new	ctccagctatcctgatactactgc	Forward primer to amplify kanMX at srs2 locus in strain 3833 to create strains 5896 and 5897. Used as forward primer to confirm 5' junction.
1565	Srs2downstreamrev_new	ggcatactgctcattcatagctg	Reverse primer to amplify kanMX at srs2 locus in strain 3833 to create strains 5896 and 5897. Used as reverse primer to confirm 3' junction in srs2::kanMX.
1742	Srs2_2506-2525F	gatttcacgtcagctgcgga	Forward primer to confirm srs2 absence in srs2::kanMX.
2469	sgs1rev375bpfrom3	cgctagactggatgacactt	Reverse primer to amplify kanMX at sgs1 locus in strain 5027 to create strains 5889 and 5890. Used to confirm presence of kanMX. Used as reverse primer for 3' junction check.
2654 or 2765	HIS for	cgtatgtgaatgctggtcgcta	Forward primer to confirm 3' junction in srs2::kanMX.
2662	Junction check upstream Rev RNH1/NAT	gagcgtttccctgctcgcag	Reverse primer to confirm 5' junction in slx8::natMX.
2663	Junction check downstream For RNH1/NAT	ctggaggtcaccaacgtcaacg	Forward primer to confirm 3' junction in slx8::natMX.
2838	pFA-Srs2-R	cggaggatgcagttcatcaa	Reverse primer to confirm srs2 absence in srs2::kanMX.
2842	Sgs1_5JxnFor_155bp_upstream	gctgggtgatcattggtgat	Forward primer to amplify kanMX at sgs1 locus in strain 5027 to create strains 5889 and 5890. Used to confirm presence of kanMX. Used as forward primer for 5' junction check.

3107	2Step_pAG32_F	ggtcagggcctcagcctggccgaaa	Forward primer to amplify CAG repeat in localization strains to confirm tract length
3108	2Step_pAG32_R	ggccggcggaacggggctcgaa	Reverse primer to amplify CAG repeat in localization strains to confirm tract length
3177	HIS5-check-insert-upstream	tgtgaatgctggtcgctata	Forward primer to confirm 3' junction in sgs1::kanMX.
3369	mVenus-gibson-for	cccagagaagaagacgagggtggttccggtggttccatgtctaaaggtgaagaattattc	Forward primer to amplify mVenus fragment for Gibson assembly. Contains 20bp homology to the Rad51 sequence (excluding the stop codon), a GGSGGS amino acid linker sequence, and the primer sequence annealing to the mVenus fragment.
3370	mVenus-gibson-rev	agagacaagagaccaaatacttatttgtacaattcatccatacc	Reverse primer to amplify mVenus fragment for Gibson assembly. Contains 20bp homology to the Rad51 sequence (excluding the stop codon), and the primer sequence annealing to the mVenus fragment.
3371	Rad51-P693-for	gtatttggtctcttgtctct	Forward primer to amplify Rad51 fragment excluding the stop codon for Gibson assembly.
3372	Rad51-P693-rev	ctcgtcttcttctctggg	Reverse primer to amplify Rad51 fragment excluding the stop codon for Gibson assembly.
3373	Rad51-mVenus-junctionCheck_for	gcacattcttccaccacgc	Forward primer used to confirm correct junction in Rad51-mVenus plasmid assembly.
3374	Rad51-mVenus-junctionCheck_rev	cagctctggtcttgtagttacc	Reverse primer used to confirm correct junction in Rad51-mVenus plasmid assembly.
3375	mVenus-flanking-junctionCheck_for	gatccaaacgaaaagagagacc	Forward primer used to confirm correct junction in Rad51-mVenus plasmid assembly.
3376	mVenus-flanking-junctionCheck_rev	aggaggaagtagtcatcggg	Reverse primer used to confirm correct junction in Rad51-mVenus plasmid assembly.

Supplemental Figure 1. Wildtype Cells: CAG Repeat Locus at NPC and Colocalized

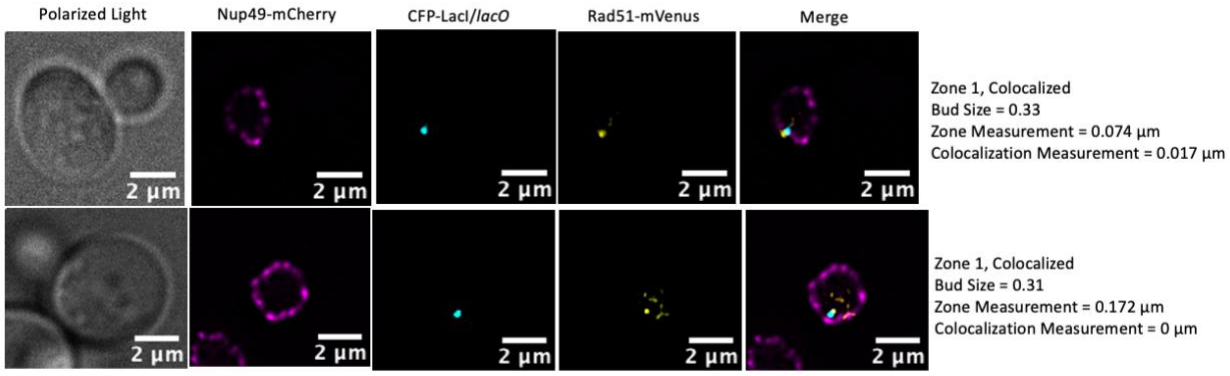

Supplemental Figure 2. Wildtype Cells: CAG Repeat Locus at NPC and Not Colocalized

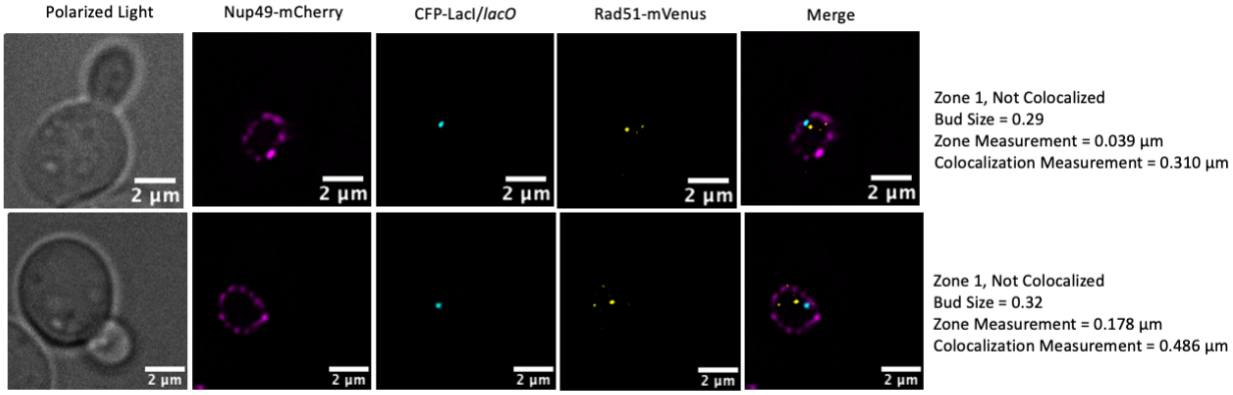

Supplemental Figure 3. Wildtype Cells: CAG Repeat Locus Not at NPC and Not Colocalized

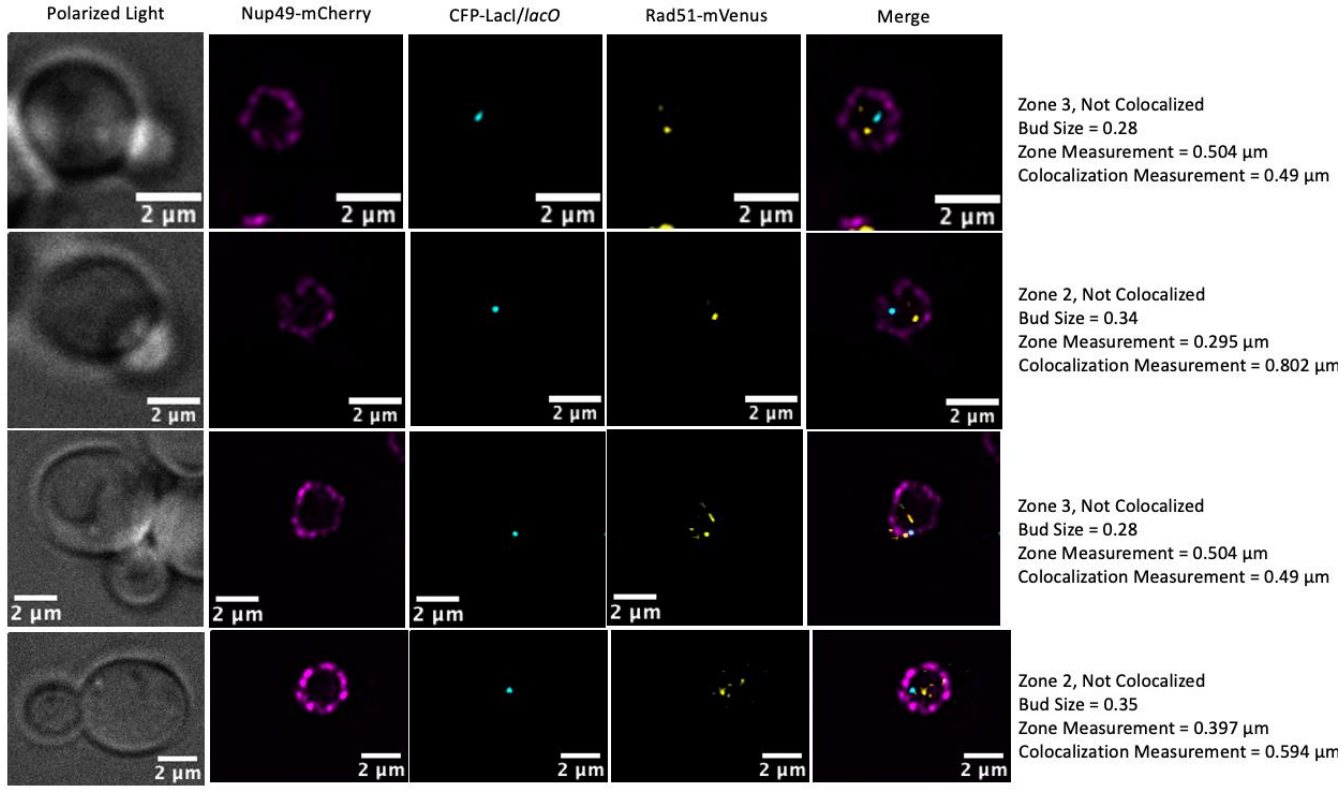

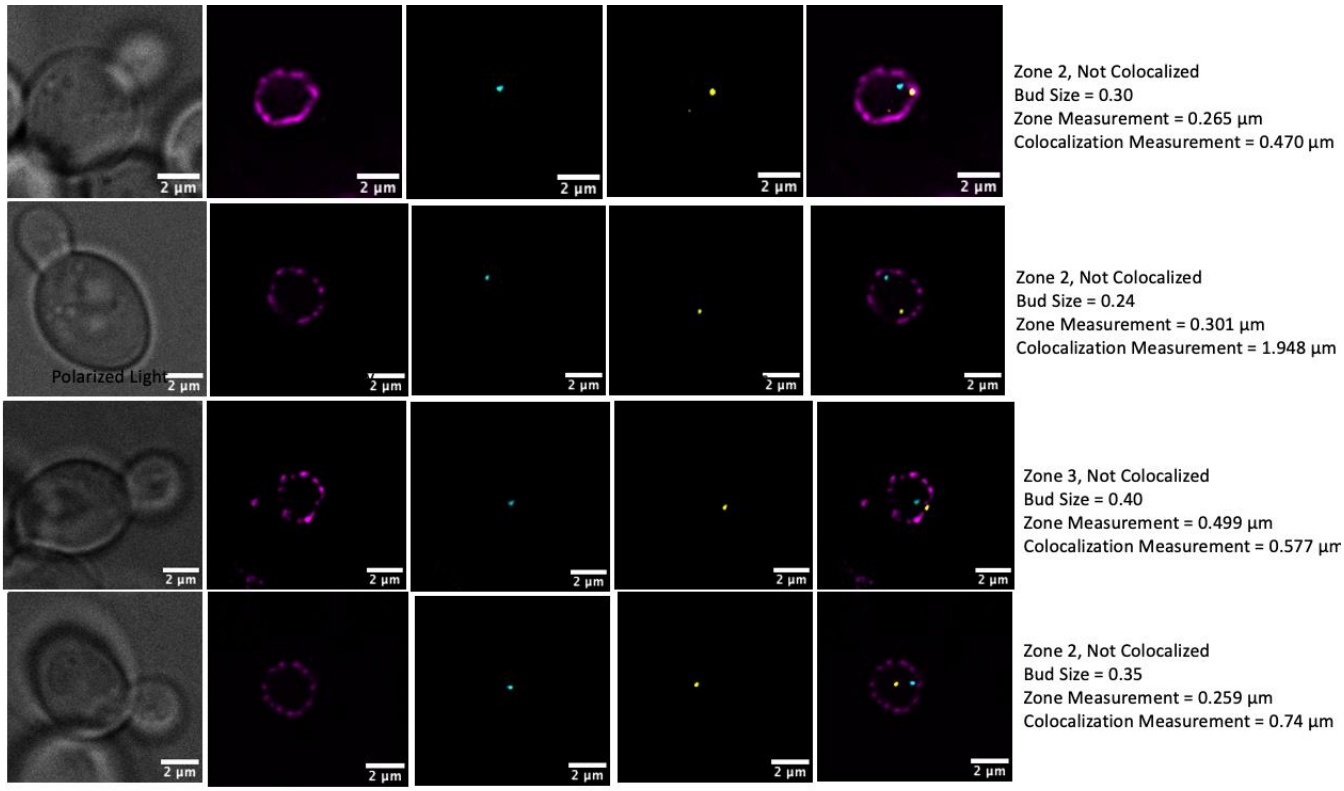

Zone 2, Not Colocalized
Bud Size = 0.30
Zone Measurement = 0.265 µm
Colocalization Measurement = 0.470 µm

Zone 2, Not Colocalized
Bud Size = 0.24
Zone Measurement = 0.301 µm
Colocalization Measurement = 1.948 µm

Zone 3, Not Colocalized
Bud Size = 0.40
Zone Measurement = 0.499 µm
Colocalization Measurement = 0.577 µm

Zone 2, Not Colocalized
Bud Size = 0.35
Zone Measurement = 0.259 µm
Colocalization Measurement = 0.74 µm

Supplemental Figure 4. *slx8*Δ Cells: CAG Repeat Locus at NPC and Not Colocalized

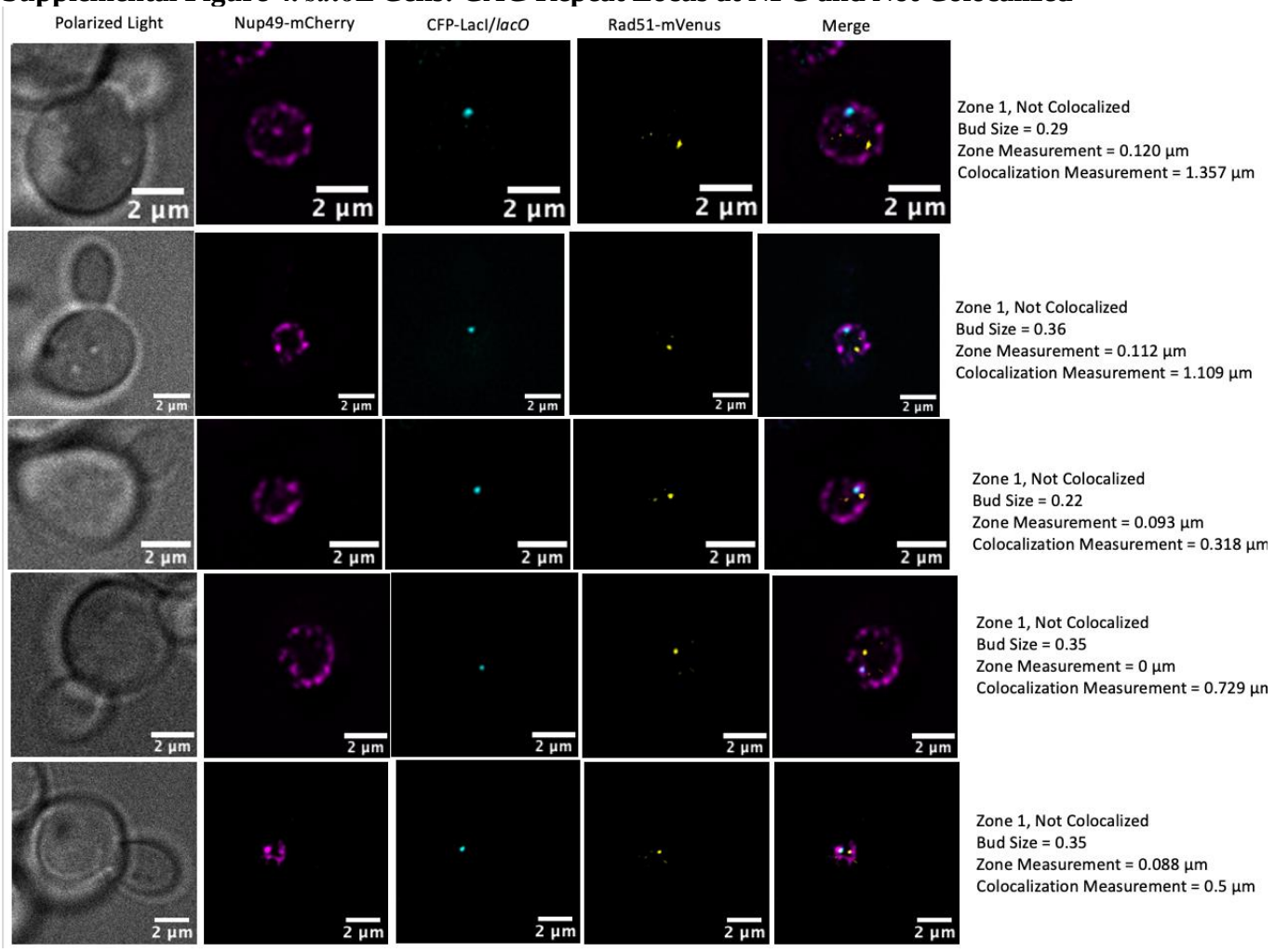

Supplemental Figure 5. *slx8*Δ Cells: CAG Repeat Locus Not at NPC and Colocalized

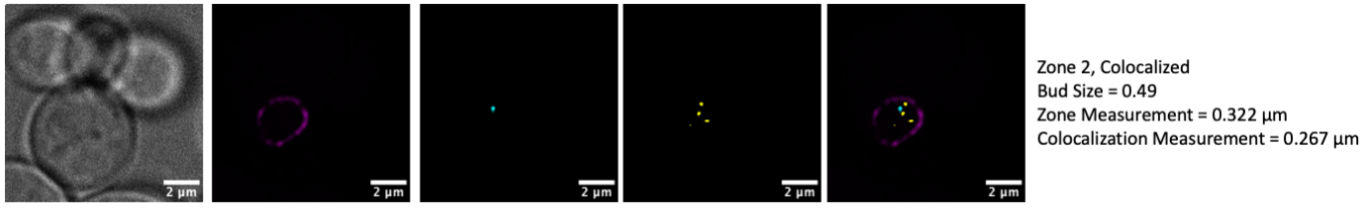

Supplemental Figure 6. *slx8*Δ Cells: CAG Repeat Locus Not at NPC and Not Colocalized

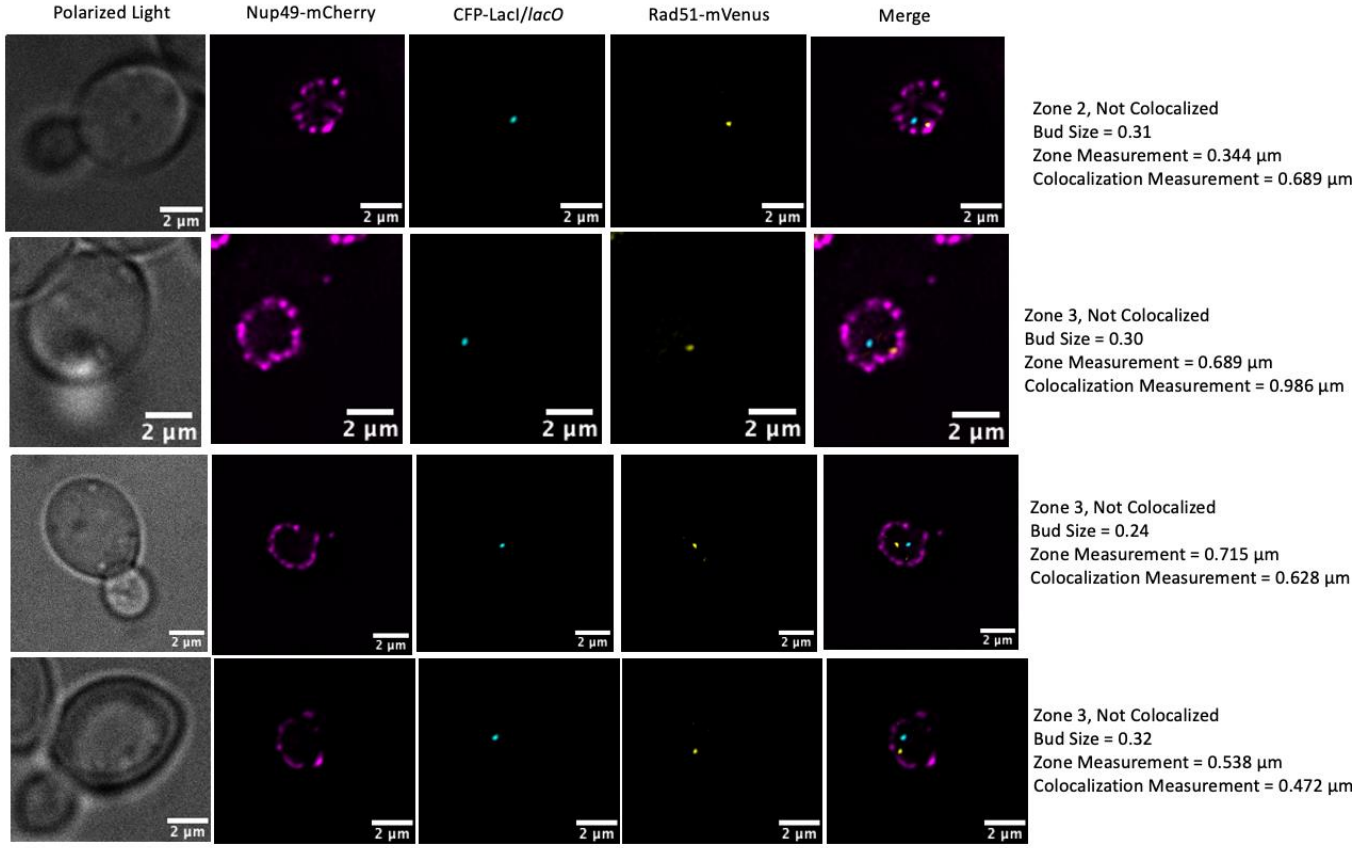

Supplemental Figure 7. *srs2*Δ Cells: CAG Repeat Locus At NPC and Colocalized

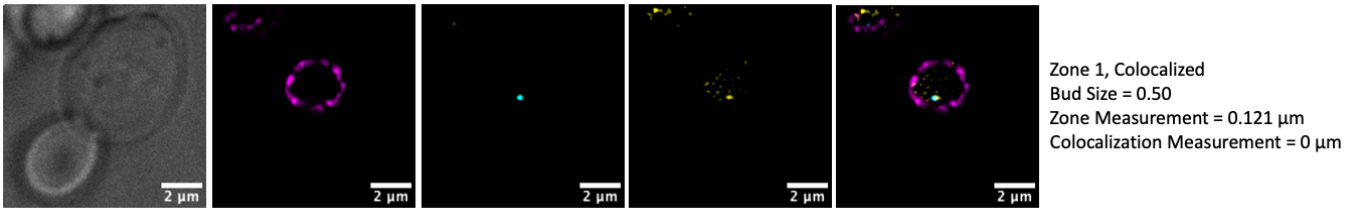

Supplemental Figure 8. *srs2*Δ Cells: CAG Repeat Locus At NPC and Not Colocalized

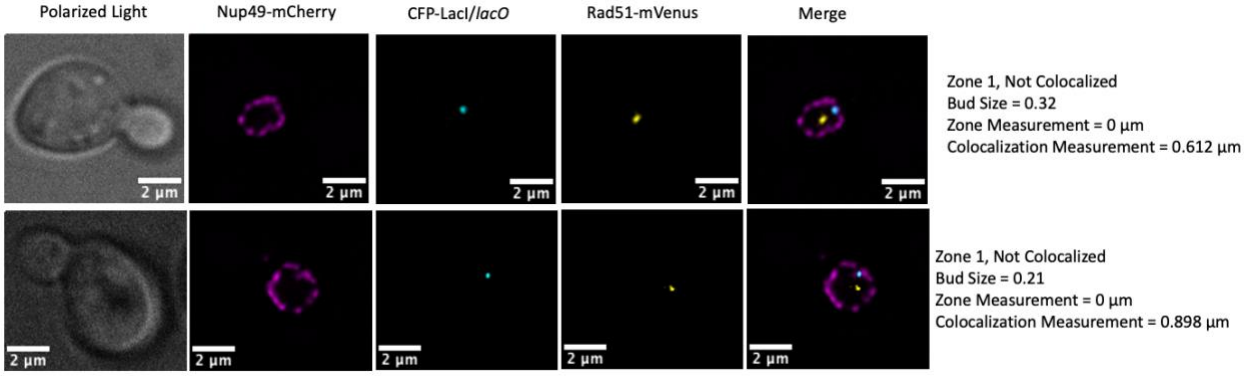

Supplemental Figure 9. *srs2*Δ Cells: CAG Repeat Locus Not At NPC and Colocalized

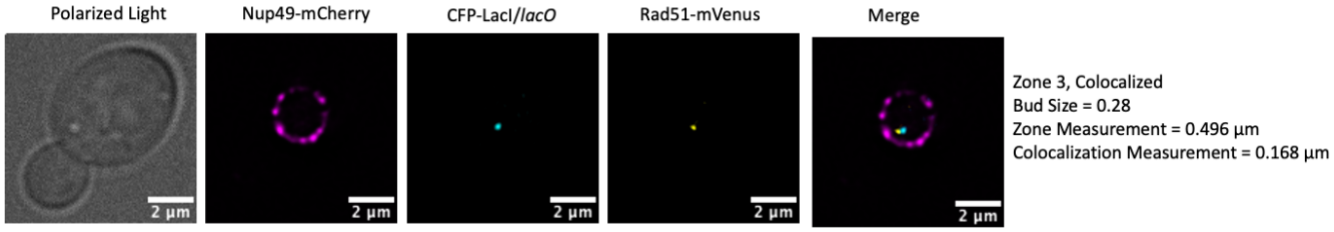

Supplemental Figure 10. *srs2*Δ Cells: CAG Repeat Locus Not At NPC and Not Colocalized

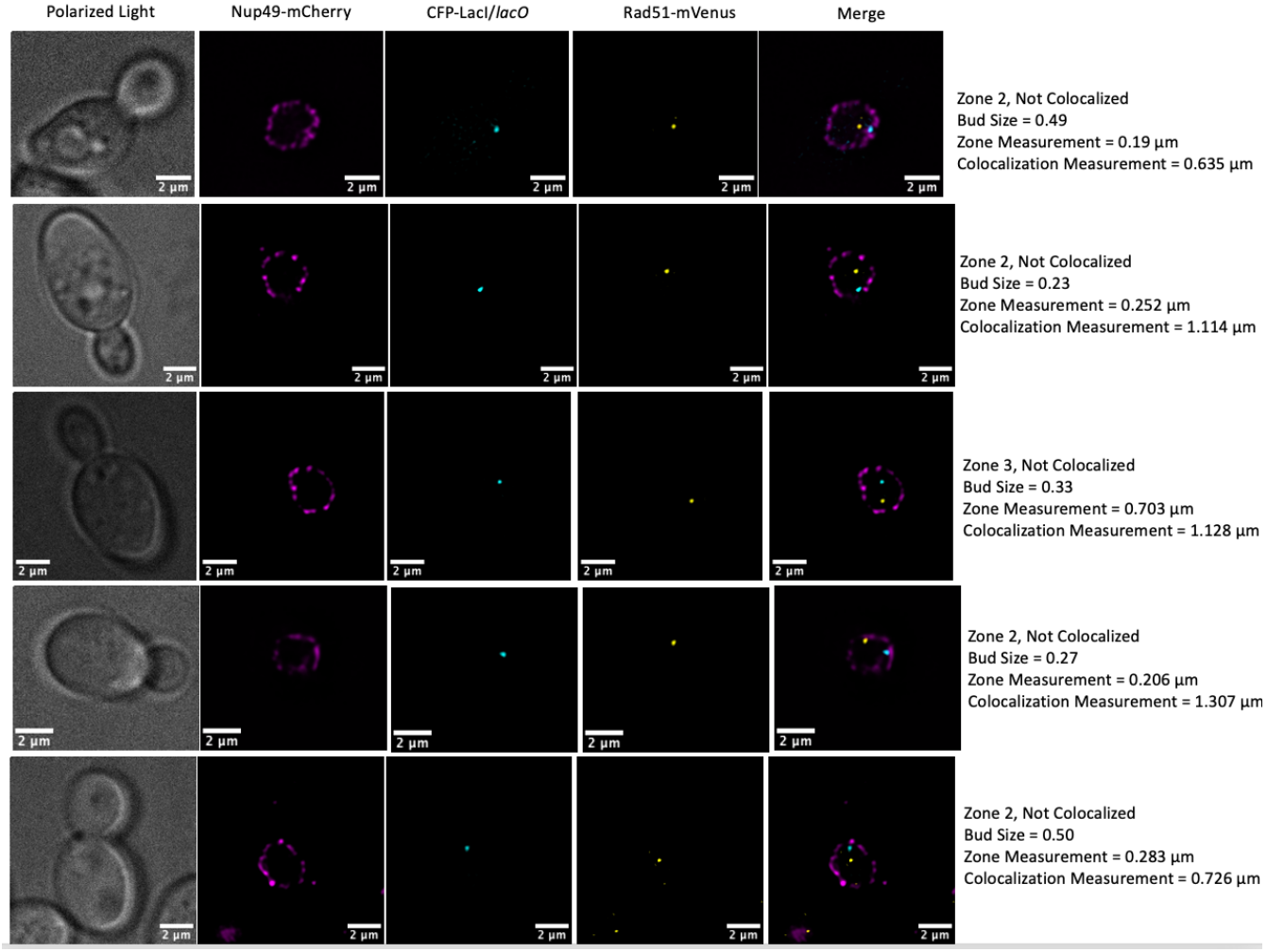

Supplemental Figure 11. *sgs1*Δ Cells: CAG repeat locus at NPC and Colocalized

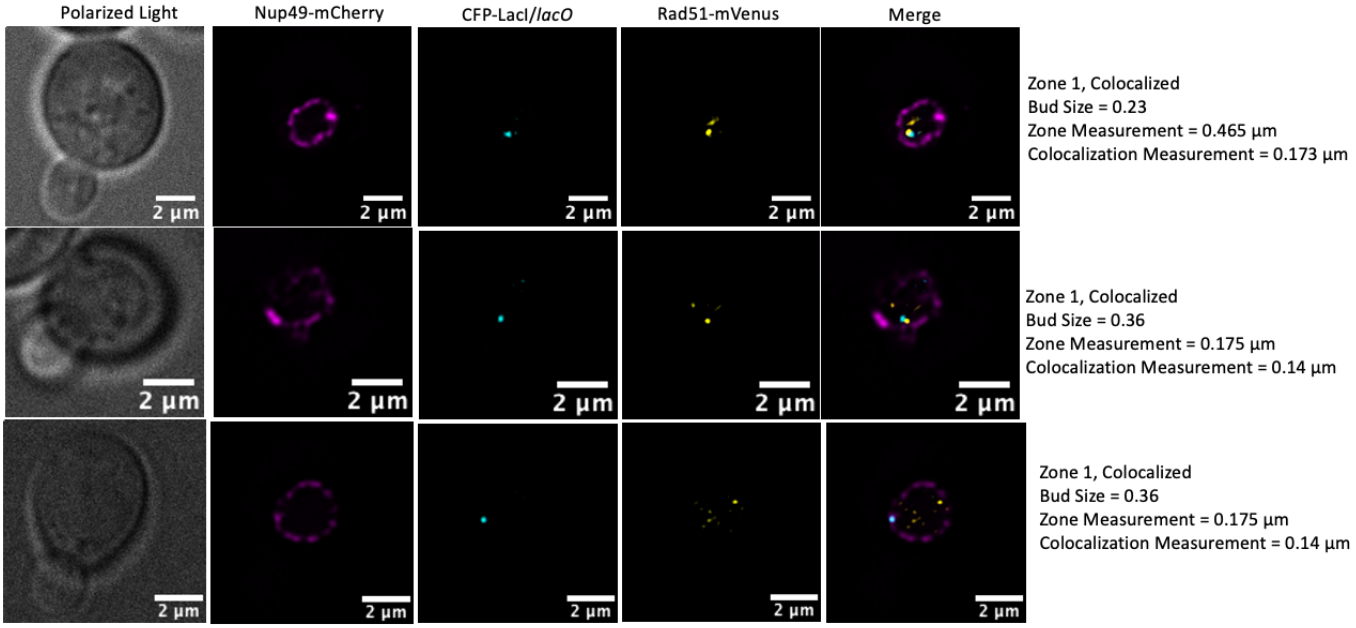

Supplemental Figure 12. *sgs1*Δ Cells: CAG repeat locus at NPC and Not Colocalized

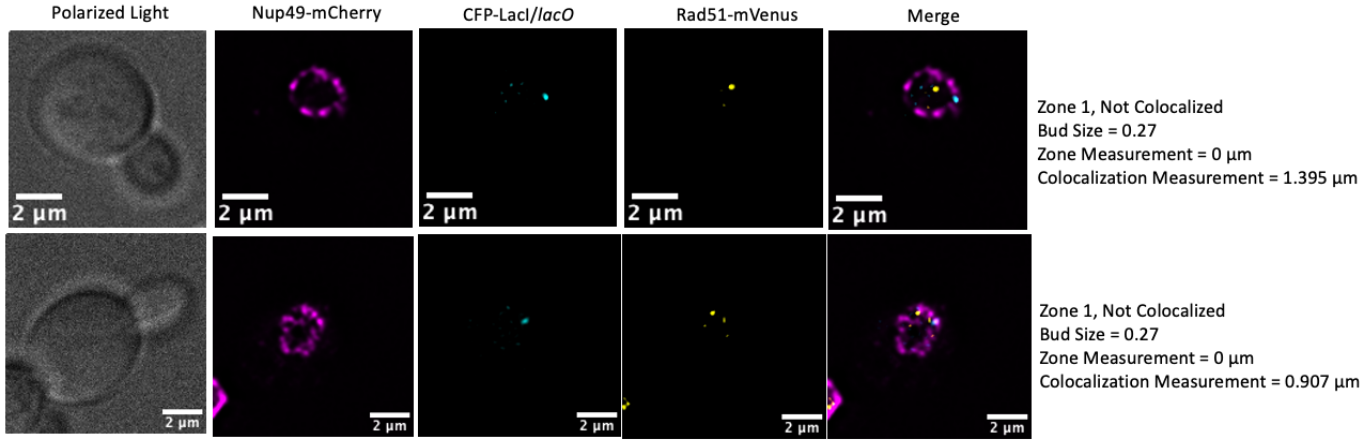

Supplemental Figure 13. MMS Sensitivity Spot Assay

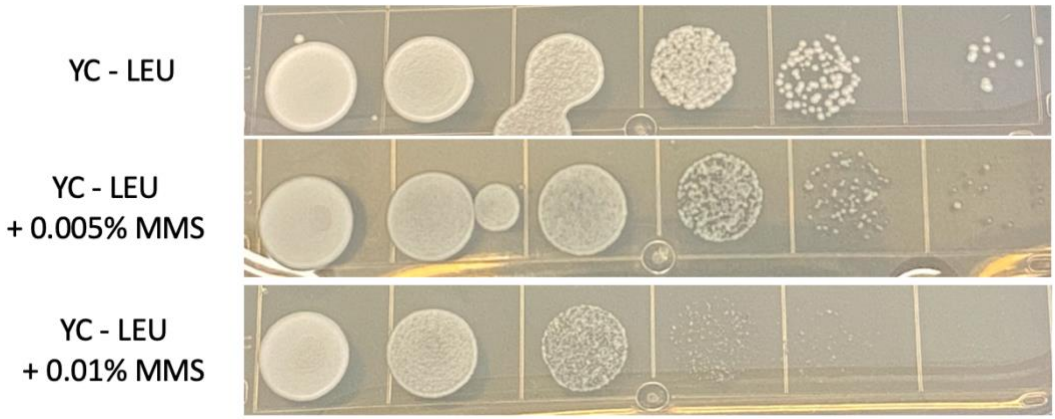

Growth on YC-Leucine media containing no MMS, 0.005% MMS, and 0.01% MMS. Assay shown depicts strain 5853 (Wildtype strain containing CFP-LacI/*lacO*, Nup49-mCherry, and Rad51-mVenus plasmid). Single colonies were suspended in 150 µL deionized water, serially diluted 10-fold six times, and 30 µL of each suspension was plated. Cells were grown at 30ºC for two days.

References

Antony, E., Tomko, E. J., Xiao, Q., Krejci, L., Lohman, T. M., & Ellenberger, T. (2009). Srs2 Disassembles Rad51 Filaments by a Protein-Protein Interaction Triggering ATP Turnover and Dissociation of Rad51 from DNA. *Molecular Cell*, *35*(1), 105–115. https://doi.org/10.1016/j.molcel.2009.05.026

Arras, S. D. M., Hibbard, T. R., Mitsugi-McHattie, L., Woods, M. A., Johnson, C. E., Munkacsi, A., Denmat, S. H.-L., & Ganley, A. R. D. (2020). *Creeping yeast: A simple, cheap, and robust protocol for the identification of mating type in* Saccharomyces cerevisiae [Preprint]. Microbiology. https://doi.org/10.1101/2020.01.19.911990

Bhargava, R., Onyango, D. O., & Stark, J. M. (2016). Regulation of Single-Strand Annealing and its Role in Genome Maintenance. *Trends in Genetics*, *32*(9), 566–575. https://doi.org/10.1016/j.tig.2016.06.007

Böhm, S., Mihalevic, M. J., Casal, M. A., & Bernstein, K. A. (2015). Disruption of SUMO-targeted ubiquitin ligases Slx5–Slx8/RNF4 alters RecQ-like helicase Sgs1/BLM localization in yeast and human cells. *DNA Repair*, *26*, 1–14. https://doi.org/10.1016/j.dnarep.2014.12.004

Branzei, D., & Foiani, M. (2005). The DNA damage response during DNA replication. *Current Opinion in Cell Biology*, *17*(6), 568–575. https://doi.org/10.1016/j.ceb.2005.09.003

Branzei, D., Sollier, J., Liberi, G., Zhao, X., Maeda, D., Seki, M., Enomoto, T., Ohta, K., & Foiani, M. (2006). Ubc9- and Mms21-Mediated Sumoylation Counteracts Recombinogenic Events at Damaged Replication Forks. *Cell*, *127*(3), 509–522. https://doi.org/10.1016/j.cell.2006.08.050

Burgess, R. C., Rahman, S., Lisby, M., Rothstein, R., & Zhao, X. (2007). The Slx5-Slx8 Complex Affects Sumoylation of DNA Repair Proteins and Negatively Regulates Recombination. *Molecular and Cellular Biology*, *27*(17), 6153–6162. https://doi.org/10.1128/MCB.00787-07

Crickard, J. B., Xue, C., Wang, W., Kwon, Y., Sung, P., & Greene, E. C. (2019). The RecQ helicase Sgs1 drives ATP-dependent disruption of Rad51 filaments. *Nucleic Acids Research*, *47*(9), 4694–4706. https://doi.org/10.1093/nar/gkz186

Da Ines, O., Degroote, F., Goubely, C., Amiard, S., Gallego, M. E., & White, C. I. (2013). Meiotic Recombination in Arabidopsis Is Catalysed by DMC1, with RAD51 Playing a Supporting Role. *PLoS Genetics*, *9*(9), e1003787. https://doi.org/10.1371/journal.pgen.1003787

Davis, A. (2003). The Rad52–Rad59 complex interacts with Rad51 and replication protein A. *DNA Repair*, *2*(10), 1127–1134. https://doi.org/10.1016/S1568-7864(03)00121-6

Dhingra, N., Kuppa, S., Wei, L., Pokhrel, N., Baburyan, S., Meng, X., Antony, E., & Zhao, X. (2021). The Srs2 helicase dampens DNA damage checkpoint by recycling RPA from chromatin. *Proceedings of the National Academy of Sciences*, *118*(8), e2020185118. https://doi.org/10.1073/pnas.2020185118

Dhingra, N., Wei, L., & Zhao, X. (2019). Replication protein A (RPA) sumoylation positively influences the DNA damage checkpoint response in yeast. *Journal of Biological Chemistry*, *294*(8), 2690–5388. https://doi.org/10.1074/jbc.RA118.006006

Esta, A., Ma, E., Dupaigne, P., Maloisel, L., Guerois, R., Le Cam, E., Veaute, X., & Coïc, E. (2013). Rad52 Sumoylation Prevents the Toxicity of Unproductive Rad51 Filaments

Independently of the Anti-Recombinase Srs2. *PLoS Genetics*, *9*(10), e1003833. https://doi.org/10.1371/journal.pgen.1003833

Freudenreich, C. H., Kantrow, S. M., & Zakian, V. A. (1998). Expansion and Length-Dependent Fragility of CTG Repeats in Yeast. *Science*, *279*(5352), 853–856. https://doi.org/10.1126/science.279.5352.853

Gietz, R. D., & Schiestl, R. H. (2007). High-efficiency yeast transformation using the LiAc/SS carrier DNA/PEG method. *Nature Protocols*, *2*(1), 31–34. https://doi.org/10.1038/nprot.2007.13

Jakupciak, J. P., & Wells, R. D. (1999). Genetic instabilities in (CTG.CAG) repeats occur by recombination. *The Journal of Biological Chemistry*, *274*(33), 23468–23479. https://doi.org/10.1074/jbc.274.33.23468

Johnson, E. S. (2004). Protein Modification by SUMO. *Annual Review of Biochemistry*, *73*(1), 355–382. https://doi.org/10.1146/annurev.biochem.73.011303.074118

Karim, A. S., Curran, K. A., & Alper, H. S. (2013). Characterization of plasmid burden and copy number in *Saccharomyces cerevisiae* for optimization of metabolic engineering applications. *FEMS Yeast Research*, *13*(1), 107–116. https://doi.org/10.1111/1567-1364.12016

Khadaroo, B., Teixeira, M. T., Luciano, P., Eckert-Boulet, N., Germann, S. M., Simon, M. N., Gallina, I., Abdallah, P., Gilson, E., Géli, V., & Lisby, M. (2009). The DNA damage response at eroded telomeres and tethering to the nuclear pore complex. *Nature Cell Biology*, *11*(8), 980–987. https://doi.org/10.1038/ncb1910

Kolesar, P., Sarangi, P., Altmannova, V., Zhao, X., & Krejci, L. (2012). Dual roles of the SUMO-interacting motif in the regulation of Srs2 sumoylation. *Nucleic Acids Research*, *40*(16), 7831–7843. https://doi.org/10.1093/nar/gks484

Kowalczykowski, S. C. (1998). DNA strand exchange proteins a biochemical and physical comparison. *Frontiers in Bioscience*, *3*(4), d570-603. https://doi.org/10.2741/A304

Kremers, G.-J., Goedhart, J., van Munster, E. B., & Gadella, T. W. J. (2006). Cyan and Yellow Super Fluorescent Proteins with Improved Brightness, Protein Folding, and FRET Förster Radius ˚. *Biochemistry*, *45*(21), 6570–6580. https://doi.org/10.1021/bi0516273

Lambert, S., Watson, A., Sheedy, D. M., Martin, B., & Carr, A. M. (2005). Gross Chromosomal Rearrangements and Elevated Recombination at an Inducible Site-Specific Replication Fork Barrier. *Cell*, *121*(5), 689–702. https://doi.org/10.1016/j.cell.2005.03.022

López Castel, A., Cleary, J. D., & Pearson, C. E. (2010). Repeat instability as the basis for human diseases and as a potential target for therapy. *Nature Reviews Molecular Cell Biology*, *11*(3), 165–170. https://doi.org/10.1038/nrm2854

Malkova, A., Ivanov, E. L., & Haber, J. E. (1996). Double-strand break repair in the absence of RAD51 in yeast: A possible role for break-induced DNA replication. *Proceedings of the National Academy of Sciences*, *93*(14), 7131–7136. https://doi.org/10.1073/pnas.93.14.7131

Meister, P., Gehlen, L. R., Varela, E., Kalck, V., & Gasser, S. M. (2010). Visualizing Yeast Chromosomes and Nuclear Architecture. In *Methods in Enzymology* (Vol. 470, pp. 535–567). Elsevier. https://doi.org/10.1016/S0076-6879(10)70021-5

Nagai, S., Dubrana, K., Tsai-Pflugfelder, M., Davidson, M. B., Roberts, T. M., Brown, G. W., Varela, E., Hediger, F., Gasser, S. M., & Krogan, N. J. (2008). Functional Targeting of

DNA Damage to a Nuclear Pore-Associated SUMO-Dependent Ubiquitin Ligase. *Science*, *322*(5901), 597–602. https://doi.org/10.1126/science.1162790

Ohshima, K., & Wells, R. D. (1997). Hairpin Formation during DNA Synthesis Primer Realignmentin Vitro in Triplet Repeat Sequences from Human Hereditary Disease Genes. *Journal of Biological Chemistry*, *272*(27), 16798–16806. https://doi.org/10.1074/jbc.272.27.16798

Oza, P., Jaspersen, S. L., Miele, A., Dekker, J., & Peterson, C. L. (2009). Mechanisms that regulate localization of a DNA double-strand break to the nuclear periphery. *Genes & Development*, *23*(8), 912–927. https://doi.org/10.1101/gad.1782209

Pelletier, R., Krasilnikova, M. M., Samadashwily, G. M., Lahue, R., & Mirkin, S. M. (2003). Replication and Expansion of Trinucleotide Repeats in Yeast. *Molecular and Cellular Biology*, *23*(4), 1349–1357. https://doi.org/10.1128/MCB.23.4.1349-1357.2003

Pfander, B., Moldovan, G.-L., Sacher, M., Hoege, C., & Jentsch, S. (2005). SUMO-modified PCNA recruits Srs2 to prevent recombination during S phase. *Nature*, *436*(7049), 428–433. https://doi.org/10.1038/nature03665

Prasher, D. C., Eckenrode, V. K., Ward, W. W., Prendergast, F. G., & Cormier, M. J. (1992). Primary structure of the Aequorea victoria green-fluorescent protein. *Gene*, *111*(2), 229–233. https://doi.org/10.1016/0378-1119(92)90691-H

Reddy, P. S., & Housman, D. E. (1997). The complex pathology of trinucleotide repeats. *Current Opinion in Cell Biology*, *9*(3), 364–372. https://doi.org/10.1016/S0955-0674(97)80009-9

Robinett, C. C., Straight, A., Li, G., Willhelm, C., Sudlow, G., Murray, A., & Belmont, A. S. (1996). In vivo localization of DNA sequences and visualization of large-scale chromatin

organization using lac operator/repressor recognition. *Journal of Cell Biology*, *135*(6), 1685–1700. https://doi.org/10.1083/jcb.135.6.1685

Sacher, M., Pfander, B., Hoege, C., & Jentsch, S. (2006). Control of Rad52 recombination activity by double-strand break-induced SUMO modification. *Nature Cell Biology*, *8*(11), 1284–1290. https://doi.org/10.1038/ncb1488

Samadashwily, G. M., Raca, G., & Mirkin, S. M. (1997). Trinucleotide repeats affect DNA replication in vivo. *Nature Genetics*, *17*(3), 298–304. https://doi.org/10.1038/ng1197-298

Sheff, M. A., & Thorn, K. S. (2004). Optimized cassettes for fluorescent protein tagging inSaccharomyces cerevisiae. *Yeast*, *21*(8), 661–670. https://doi.org/10.1002/yea.1130

Su, X. A., Dion, V., Gasser, S. M., & Freudenreich, C. H. (2015). Regulation of recombination at yeast nuclear pores controls repair and triplet repeat stability. *Genes & Development*, *29*(10), 1006–1017. https://doi.org/10.1101/gad.256404.114

Twomey, E. C., Ji, Z., Wales, T. E., Bodnar, N. O., Ficarro, S. B., Marto, J. A., Engen, J. R., & Rapoport, T. A. (2019). Substrate processing by the Cdc48 ATPase complex is initiated by ubiquitin unfolding. *Science*, *365*(6452), eaax1033. https://doi.org/10.1126/science.aax1033

Waterman, D. P., Zhou, F., Li, K., Lee, C.-S., Tsabar, M., Eapen, V. V., Mazzella, A., & Haber, J. E. (2019). Live cell monitoring of double strand breaks in S. cerevisiae. *PLOS Genetics*, *15*(3), e1008001. https://doi.org/10.1371/journal.pgen.1008001

Whalen, J. M., Dhingra, N., Wei, L., Zhao, X., & Freudenreich, C. H. (2020). Relocation of Collapsed Forks to the Nuclear Pore Complex Depends on Sumoylation of DNA Repair Proteins and Permits Rad51 Association. *Cell Reports*, *31*(6), 107635. https://doi.org/10.1016/j.celrep.2020.107635